

Searching for Compton-thick active galactic nuclei at $z \sim 0.1$

A.D. Goulding¹; D.M. Alexander¹; J.R. Mullaney¹; J.M. Gelbord^{1,2}; R.C. Hickox¹; M. Ward¹ & M.G. Watson³

¹*Department of Physics, Durham University, South Road, Durham.*

²*Department of Astronomy and Astrophysics, 525 Davey Laboratory, The Pennsylvania State University, University Park, PA 16802.*

³*Department of Physics & Astronomy, University of Leicester, Leicester, LE1 7RH, UK*

Released 2010 Xxxxx XX

ABSTRACT

Using a suite of X-ray, mid-infrared (IR) and optical active galactic nuclei (AGN) luminosity indicators, we search for Compton-thick AGNs with intrinsic $L_X > 10^{42}$ erg s⁻¹ at $z \sim 0.03$ – 0.2 , a region of parameter space which is currently poorly constrained by deep narrow-field and high-energy ($E > 10$ keV) all-sky X-ray surveys. We have used the widest *XMM-Newton* survey (the serendipitous source catalogue) to select a representative sub-sample (14; ≈ 10 percent) of the 147 X-ray undetected candidate Compton-thick AGNs in the Sloan Digital Sky Survey (SDSS) with $f_X/f_{[\text{OIII}]}$ < 1; the 147 sources account for ≈ 50 percent of the overall Type-2 AGN population in the SDSS–*XMM* overlap region. We use mid-IR spectral decomposition analyses and emission-line diagnostics, determined from pointed *Spitzer*-IRS spectroscopic observations of these candidate Compton-thick AGNs, to estimate the intrinsic AGN emission (predicted 2–10 keV X-ray luminosities, $L_X \approx (0.2\text{--}30) \times 10^{42}$ erg s⁻¹). On the basis of the optical [OIII], mid-IR [OIV] and 6 μm AGN continuum luminosities we conservatively find that the X-ray emission in at least 6/14 ($\gtrsim 43$ percent) of our sample appear to be obscured by Compton-thick material with $N_H > 1.5 \times 10^{24}$ cm⁻². Under the reasonable assumption that our 14 AGNs are representative of the overall X-ray undetected AGN population in the SDSS–*XMM* parent sample, we find that $\gtrsim 20$ percent of the optical Type-2 AGN population are likely to be obscured by Compton-thick material. This implies a space-density of $\log(\Phi) \gtrsim -4.9$ Mpc⁻³ for Compton-thick AGNs with $L_X \gtrsim 10^{42}$ erg s⁻¹ at $z \sim 0.1$, which we suggest may be consistent with that predicted by X-ray background synthesis models. Furthermore, using the 6 μm continuum luminosity to infer the intrinsic AGN luminosity and the stellar velocity dispersion to estimate M_{BH} , we find that the most conservatively identified Compton-thick AGNs in this sample may harbour some of the most rapidly growing black holes (median $M_{\text{BH}} \approx 3 \times 10^7 M_\odot$) in the nearby Universe, with a median Eddington ratio of $\eta \approx 0.2$.

Key words: galaxies: active – galaxies: evolution – galaxies: nuclei – infrared: galaxies

1 INTRODUCTION

There is now strong observational evidence that all massive galaxies ($M_* \approx 10^{10}$ – $10^{12} M_\odot$) in the nearby Universe host a central supermassive black hole (SMBH; $M_{\text{BH}} \approx 10^6$ – $10^9 M_\odot$; Kormendy & Richstone 1995). These SMBHs have grown through mass accretion events (e.g., Soltan 1982; Rees 1984), during so-called active galactic nucleus (AGN) phases. The seminal discovery that the masses of SMBHs are proportional to those of their stellar spheroids implies a strong physical association between AGN activity and galaxy evolution (e.g., Magorrian et al.

1998; Ferrarese & Merritt 2000; Gebhardt et al. 2000; Tremaine et al. 2002). To fully interpret the role played by AGN in this symbiosis requires a complete census of obscured and unobscured AGNs across cosmic time.

Unbiased deep and wide-field X-ray surveys have been instrumental in the identification of a large proportion of the AGN population to high redshifts ($z \sim 5$; e.g., Alexander et al. 2001; Barger et al. 2003; Fiore et al. 2003; Tozzi et al. 2006; Brusa et al. 2010). Using the exceptional sensitivities of *XMM-Newton* and the *Chandra X-ray Observatory*, > 80 per cent of the X-ray background (XRB) has been resolved into discrete sources at soft energies (0.5–

5 keV; e.g., Worsley et al. 2005; Hickox & Markevitch 2006, 2007). However, AGN synthesis models for the XRB predict that ~ 50 per cent of the AGN population may be heavily obscured and remains undetected at $E > 6$ keV in deep X-ray surveys (e.g., Gilli et al. 2007; Treister et al. 2009).

Using high-quality X-ray spectroscopic analyses of objects in the local Universe, it is now well-established that the majority of AGNs are obscured along the line-of-sight by large columns of gas and dust (e.g., Risaliti et al. 1999; Matt et al. 2000). The presence of this obscuring material results in strongly depressed nuclear X-ray emission observed at $E \sim 0.5\text{--}10$ keV. For those AGNs with column densities exceeding the inverse Thomson cross-section ($N_H \sim 1.5 \times 10^{24} \text{ cm}^{-2}$; i.e., Compton-thick absorption) very few photons are detected at $E < 10$ keV due to significant absorption and scattering. Moreover, for sources with $N_H > 10^{25} \text{ cm}^{-2}$, the entire high energy spectrum is down-scattered and, eventually, absorbed by the heavily Compton-thick material. Consequently, the observed X-ray flux in Compton-thick AGNs is often rendered so weak that it becomes comparable to the X-ray emission arising from the host-galaxy, making their detection extremely difficult. The direct identification of mildly Compton-thick AGNs ($N_H \sim (1.5\text{--}10) \times 10^{24} \text{ cm}^{-2}$) is possible through X-ray observations at $E > 10$ keV (e.g., using *Beppo-SAX*, *Swift*, *Suzaku*) where the relatively unabsorbed high-energy emission can be detected. However, the sensitivities of current $E > 10$ keV observatories are substantially limited by high backgrounds, poor effective areas and inadequate spatial resolutions. Indeed, to date, only 18 Compton-thick AGNs have been unambiguously identified in the Universe at $E > 10$ keV, mainly at $z \lesssim 0.01$ (for a recent review, see Della Ceca et al. 2008).

In the absence of higher-energy $E > 10$ keV data, the presence of a Compton-thick AGN may still be inferred using indirect methods: (1) from the detection of a high equivalent width (> 1 keV) Fe K_α fluorescence line at $E \sim 6.4$ keV (e.g., Awaki et al. 1991), and/or (2) nuclear emission which has been reflected into the line-of-sight by the highly ionised optically-thick material (a so-called, Compton-reflection component; e.g., Ghisellini et al. 1994; Matt et al. 1996). However, the detection of either of these Compton-thick AGN signatures is still difficult due to the required high sensitivity of the X-ray data (spectra containing $\gtrsim 200$ counts). For example, given the faint X-ray fluxes, even at low redshifts ($z \sim 0.05$), long exposure times with the most sensitive X-ray observatories (of the order 100s of kiloseconds with *Chandra* and *XMM-Newton*) are required to detect Fe K_α at a high significance. Indeed, only a further ≈ 30 local ($z < 0.01$) AGNs have been robustly determined to be Compton-thick AGNs in the absence of $E > 10$ keV data (see Comastri 2004; Della Ceca et al. 2008 and references there-in). Hence, although Compton-thick AGNs are predicted to comprise a large proportion of the overall AGN population ($\gtrsim 40$ percent; Risaliti et al. 1999; Matt et al. 2000), to date, only ≈ 50 Compton-thick AGNs have been robustly identified in the nearby Universe at $z \lesssim 0.05$ (Comastri 2004; Della Ceca et al. 2008); conversely, only ≈ 30 candidate Compton-thick AGNs (i.e., those with high EW FeK or reflection-dominated spectra) have been identified in high redshift X-ray surveys (e.g., Norman et al. 2002; Tozzi et al. 2006; Georgantopoulos et al. 2009).

Given the required X-ray sensitivity to directly identify Compton-thick AGNs using X-ray data alone, only a small fraction of the population can be discovered using current instrumentation. In recent years, new techniques have been developed to discover Compton-thick AGN candidates using complimentary wide-field optical surveys with pointed mid-infrared (IR) observations, allowing us to probe $\approx 2\text{--}3$ orders of magnitude lower in the $z\text{--}L_X$ plane than using X-ray data alone. These approaches are promising since the reprocessed mid-IR continuum emission and high-excitation optical and mid-IR narrow-line emission (i.e., [OIII] $\lambda 5007$; [Nev] $14.32 \mu\text{m}$; [Oiv] $25.89 \mu\text{m}$) in AGN are relatively unaffected by the optically-thick X-ray obscuring material in the central region and, therefore, provide reliable measurements of the intrinsic luminosity of even the most heavily Compton-thick AGNs (e.g., Heckman et al. 2005; Panessa et al. 2006; Meléndez et al. 2008; Diamond-Stanic et al. 2009; Goulding et al. 2010). For example, through examination of a local optically-selected AGN sample, Maiolino et al. (1998) and Bassani et al. (1999) find that those AGNs with X-ray-[OIII] flux ratios of $f_X/f_{[\text{OIII}]}$ < 1 almost invariably host intrinsically obscured central sources (many of which are Compton thick), and those with $f_X/f_{[\text{OIII}]} < 0.1$ always appear to be Compton thick (see also Akylas & Georgantopoulos 2009; hereafter, AG09). Furthermore, this diagnostic has successfully identified new Compton-thick AGNs which have since been unambiguously confirmed using high-quality X-ray data (e.g., NGC 5135; Levenson et al. 2004).

Clearly, indirect AGN luminosity indicators provide good first-order approximations as to whether an AGN is Compton thick. Greater reliability in identifying Compton-thick AGNs can therefore be made when considering multiple diagnostics, particularly those which probe different regions of the AGN (e.g., the emission line region and the reprocessed continuum emission). Recently, Vignali et al. (2010) combined pointed *Chandra*-ACIS observations with optical emission-line and mid-IR continuum luminosities to identify six Compton-thick quasars ($L_{[\text{OIII}]} > 2 \times 10^9 L_\odot$) at $z \sim 0.40\text{--}0.73$ in the Sloan Digital Sky Survey (SDSS). Somewhat similar approaches have also been adopted by Alexander et al. (2008); LaMassa et al. (2009); Bauer et al. (2010); Donley et al. (2010) using *Spitzer* IR spectroscopy and/or optical spectroscopy to identify high-redshift X-ray undetected Compton-thick AGNs in deep and wide-field surveys. Whilst each of these studies have successfully identified Compton-thick AGNs using multi-wavelength analyses, they sample only the most luminous systems ($L_{X,\text{intr}} \gtrsim 10^{44} \text{ erg s}^{-1}$) where the predicted space-density of Compton-thick AGNs, even at $z \sim 2$, is relatively low ($\phi \lesssim 10^{-5} \text{ Mpc}^{-3}$; Gilli et al. 2007). In order to clearly understand the evolution of these Compton-thick sources, it is vital to also identify the more modest luminosity population ($L_{X,\text{intr}} \approx [0.1\text{--}1] \times 10^{43} \text{ erg s}^{-1}$), which comprise the most energetically dominant AGNs in the nearby Universe ($z \sim 0.1$; e.g., Ueda et al. 2003; Ebrero et al. 2009; Aird et al. 2010).

In this paper, we identify a sample of nearby ($z \sim 0.03\text{--}0.2$) X-ray undetected optically selected candidate Compton-thick AGNs from a large cosmological volume which is well-matched to that of the *Chandra* Deep

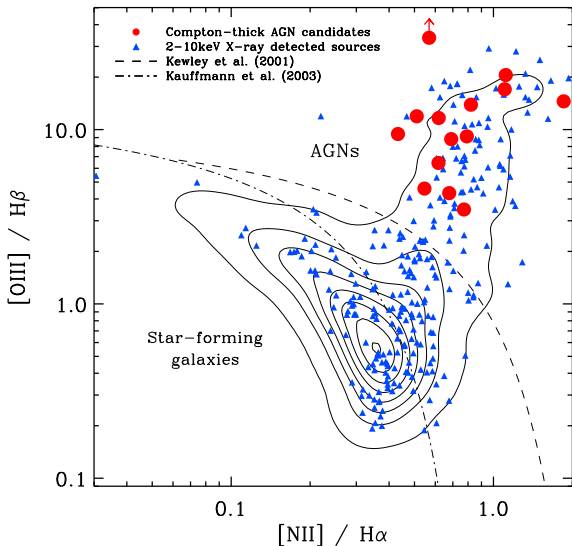


Figure 1. Optical emission line diagnostic diagram presenting the 2690 galaxies detected in the seventh data release of the Sloan Digital Sky Survey with serendipitous X-ray coverage from *XMM-Newton* at $0.03 < z < 0.2$ (solid contours). The fourteen X-ray undetected optical AGNs selected for our sample are shown with red solid circles. The 272 galaxies with hard-band X-ray detections ($E > 2$ keV) are shown with blue solid triangles. The empirical HII star-forming classification curve presented by Kauffmann et al. (2003) and the extreme starburst line of Kewley et al. (2001) are also shown with dash-dotted and dashed curves, respectively.

Fields (CDFs; Giacomoni et al. 2002; Alexander et al. 2003; Luo et al. 2008) at $z \sim 0.5$ – 2.5 (comoving volume of $V \approx 4.6 \times 10^6$ Mpc³). We use pointed high signal-to-noise *Spitzer* IR spectroscopy and 24 μ m photometry combined with the unprecedented wide-field coverage of the SDSS to explore the ubiquity of typical Compton-thick AGNs at $z \sim 0.1$. In section 2, we outline the construction of our sample of 14 optical narrow-line AGNs derived from the population of galaxies in the SDSS which lie in the large overlap region with the *XMM-Newton* Serendipitous Survey (≈ 100 deg²). These AGNs are all undetected to faint flux limits in $E \sim 2$ – 12 keV *XMM-Newton* observations, and based on their X-ray–[OIII] flux ratio limits are likely to be heavily obscured (and possibly Compton thick). In section 3, we discuss the data reduction techniques for our *Spitzer* observations and present mid-IR AGN–starburst spectral decompositions to understand both the properties of the host galaxies and the central source in these obscured AGNs. In section 4, we use mid-IR narrow-line emission and AGN-produced mid-IR continuum emission to determine the intrinsic luminosity of the obscured AGNs. We combine each of these AGN luminosity indicators in order to reliably identify which sources are Compton-thick AGNs. We use these results to further constrain the ubiquity of Compton-thick AGNs at $z \sim 0.1$. Throughout, we adopt a standard Λ CDM cosmology of $H_0 = 71$ km s^{−1} Mpc^{−1}, $\Omega_M = 0.30$, and $\Omega_\Lambda = 0.70$.

2 SAMPLE SELECTION

We select our candidate Compton-thick AGN sample on the basis of their optical and X-ray properties. Sources that are identified to be AGNs using traditional optical emission line diagnostics (e.g., Baldwin et al. 1981) but are undetected to faint limits in wide-field *XMM-Newton* observations (i.e., $f_X/f_{[\text{OIII}]}$ < 1) are strong candidates for containing heavily obscured AGNs (e.g., Bassani et al. 1999; Panessa & Bassani 2002; Akylas & Georgantopoulos 2009).¹ Here we provide the details behind the construction of our sample of X-ray undetected optically identified AGNs (i.e., candidate Compton-thick AGNs).

2.1 Construction of the optical–X-ray catalogue

We construct a parent sample of all optical spectroscopically identified galaxies in the ≈ 100 deg² overlap region between the seventh data release of the SDSS (Abazajian et al. 2009; hereafter SDSS-DR7) and the second source catalogue of the *XMM-Newton* Serendipitous survey (Watson et al. 2009; hereafter 2XMMi). We define the redshift range for our shallow wide-area sample based on the combined available cosmological volume in the deep 2Ms “pencil-beam” CDF-North (≈ 448 arcmin²; Alexander et al. 2003) and CDF-South (≈ 436 arcmin²; Giacomoni et al. 2002; Luo et al. 2008) surveys. At $z \sim 0.5$ – 2.5 , where the CDFs are complete towards X-ray luminous AGNs, the encompassed comoving volume is $V \sim 4.57 \times 10^6$ Mpc³, which is equivalent to the comoving volume in the redshift range of $z \sim 0.03$ – 0.2 in our SDSS-2XMMi selected sample.

2.1.1 AGN identification in the SDSS-DR7

The SDSS-DR7 is currently the largest publicly available optical spectroscopic catalogue (≈ 9830 deg²) containing 929,555 spectroscopic source redshifts.² Previous studies have used past data releases of the survey to show that through careful spectral analyses, general galaxy and AGN properties can be derived from these large datasets (e.g., Kauffmann et al. 2003; Heckman et al. 2004; Greene & Ho 2007). We select all galaxies with well detected narrow [OIII] $\lambda 5007$, H α , [NII] $\lambda 6585$ emission-lines (S/N > 5).³ All galaxies with detected broad Balmer emission lines (here defined as a full-width half maximum > 700 km s^{−1}) are removed as these sources are unlikely to be intrinsically obscured by a gas/dust-rich geometrically thick torus. AGNs which are heavily obscured are often found to be hosted in dust-rich galaxies, and thus are likely to be strongly reddened (i.e., H α –H β ratios $\gg 3.1$; e.g.,

¹ Throughout this manuscript we define *X-ray undetected* as those sources undetected in the hard band ($E > 2$ keV) unless otherwise stated.

² The SDSS-DR7 data archive server is available at <http://www.sdss.org/dr7/>

³ SDSS spectra are obtained through 3 arcsecond fibers; at the median redshift of our sample ($z \sim 0.08$) this projected aperture is equivalent to a physical region of ≈ 5 kpc, and hence encompasses all of the narrow-line region emission as well as a large fraction of the host galaxy emission.

Goulding & Alexander 2009). Hence, whilst useful in unambiguously discriminating between the properties of galaxies (e.g., Kauffmann et al. 2003; Wild et al. 2010), we purposely do not limit our selection to only galaxies with well-detected H β emission. Sources are separated by classification based on their optical emission-line ratios in a traditional diagnostic diagram (hereafter, BPT diagram; e.g., Baldwin et al. 1981). We conservatively identify the narrow-line AGNs in the SDSS-DR7 as those which lie above the theoretical starburst limit of Kewley et al. (2001). See Fig. 1.

2.1.2 SDSS AGNs in the XMM-Newton footprint

The 2XMMi catalogue identifies all X-ray sources detected in the 3491 observations made during the first ≈ 8 years of *XMM-Newton* operations (Watson et al. 2009). Its unprecedented sky coverage (360 deg²) and sensitivity (median *XMM-Newton* exposures of 20–50 ks) currently provides an exceptional resource for the unbiased identification of obscured AGN activity throughout the Universe. Using an automated reduction and analysis pipeline, the 2XMMi catalogue provides source positions, exposure times, X-ray fluxes and band ratios of all detected sources which serendipitously fall within the field-of-view of previous *XMM-Newton* observations.

All sources in our SDSS parent sample are matched to 2XMMi using a 3.7 arcsecond radius, which is chosen as a good compromise between maximising source numbers and minimising the probability of spurious matches (e.g., Watson et al. 2009). The matching algorithm is restricted to sources within 14 arc-minutes of the aim point of each *XMM-Newton* observation to minimise the likelihood of spurious matches due to the degradation of the X-ray PSF far off-axis. Based on the X-ray/optical positional analysis of SDSS quasars and the 2XMMi catalogue by Watson et al. (2009), if we assume no systematic offsets, then we expect our XMM-SDSS matching to be ≈ 92 percent complete. We identify all optical sources in the 2XMMi which have 3σ detections at $E \sim 2\text{--}12$ keV using the PN detector. For all other matched sources (i.e., those which lie within the footprint of an *XMM-Newton* observation but are undetected in the hard-band of the 2XMMi catalogue), we use FLIX to compute robust 3σ (likelihood threshold of 6.6) X-ray upper-limits in this band.⁴ Using a sub-sample of the matched sources that are formally undetected in the hard band in 2XMMi, we tested the use of FLIX to provide X-ray upper-limits. Broadly, we find that the upper limits provided by FLIX are consistent with the fluxes within $\pm 3\sigma$ given by 2XMMi. For the sake of comparison with previous studies, we convert these 2–12 keV upper-limits to 2–10 keV limits assuming a powerlaw spectrum with spectral index of $\Gamma = 1.4$ where $F_\nu \propto \nu^{-(\Gamma-1)}$; $\Gamma = 1.4$ is the spectral slope of the X-ray background and similar to that of many absorbed AGNs. Our final combined parent sample of SDSS-DR7 galaxies at $z \sim 0.03\text{--}0.2$

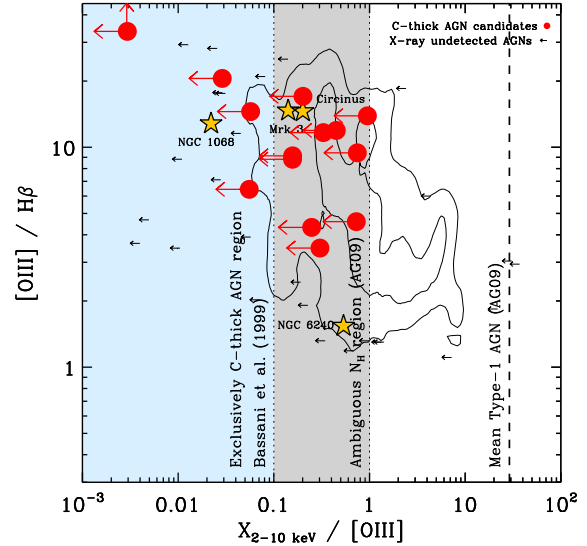


Figure 2. Intrinsic obscuration optical–X-ray diagnostic diagram for AGNs. Contours indicate the distribution of all optical AGNs in the SDSS-DR7 which lie in the *XMM-Newton* footprint (i.e., those galaxies which lie above the Kewley et al. 2001 extreme starburst line presented in Fig. 1). These contours enclose 50% and 90% of the whole X-ray undetected parent sample; outliers are shown with small arrows. We select 14 candidate Compton-thick AGNs for *Spitzer* observations based on their $f_X/f_{[\text{OIII}]}$ ratio (filled circles). Four of these sources lie in the region exclusively occupied by Compton-thick AGNs ($f_X/f_{[\text{OIII}]} < 0.1$; e.g., Bassani et al. 1999), and 10 are selected from the heavily obscured N_H region ($f_X/f_{[\text{OIII}]} \sim 0.1\text{--}1.0$) which is often found to contain Compton-thick AGNs (e.g., Bassani et al. 1999; AG09). We also show the mean Type-1 (i.e., unobscured) AGN $f_X/f_{[\text{OIII}]}$ ratio from AG09 and for comparison, four well-studied local ‘bona-fide’ Compton-thick AGNs (Circinus, Mrk 3, NGC 1068 and 6240; data is taken from Bassani et al. 1999; stars).

with complimentary hard X-ray *XMM-Newton* coverage is 2690 objects (272 are hard X-ray detected sources). The median redshift of the sample is ≈ 0.09 . Of these galaxies, 334 (≈ 12 percent) lie above the theoretical starburst limit and are classified as optical narrow-line (NL) AGNs (i.e., 101 are X-ray detected and 233 are X-ray undetected AGNs; see Fig. 1).

2.1.3 A sample of candidate Compton-thick AGNs

Assuming the optical emission-lines and X-ray AGN emission are well-correlated (e.g., Mulchaey et al. 1994; Alonso-Herrero et al. 1997), sources which are optically classified as AGNs but are undetected to faint limits in relatively deep X-ray observations are likely to be those with heavily attenuated X-ray emission, similar to the objects currently missed in deep X-ray surveys. From our well-defined parent sample of 334 optical NL AGNs, 233 are not detected in the hard-band of the 2XMMi catalogue. In this section, we outline the selection method for our sample of 14 hard-band undetected candidate Compton-thick AGNs.

The de-reddened [OIII] luminosity is assumed to be a good tracer of AGN power (e.g., Heckman et al. 2005;

⁴ FLIX is a purpose-built program provided by the *XMM-Newton* Survey Science Center. It provides robust estimates of the X-ray upper limit to a given point in the sky for a source which has not been detected in the 2XMMi catalogue. For a discussion of the upper limit algorithm see Carrera et al. (2007) and for further documentation see http://www.ledas.ac.uk/flix/flix_help.html.

Table 1. Basic source properties of the candidate Compton-thick AGNs

| ID | Source name | α_{J2000} | δ_{J2000} | z | D_L | $\log(M_{\text{BH}})$ | $\frac{[\text{OIII}]}{H\beta}$ | $\frac{[\text{NII}]}{H\alpha}$ | $\frac{H\alpha}{H\beta}$ | A_V | $\log(L_{[\text{OIII}]})$ | $\log(L_{\text{HX}})$ |
|-----|---------------------|------------------|------------------|---------|-------|-----------------------|--------------------------------|--------------------------------|--------------------------|--------|---------------------------|-------------------------|
| (1) | (2) | (deg) | (deg) | (5) | (Mpc) | (M_\odot) | (8) | (9) | (10) | (mags) | (erg s^{-1}) | (erg s^{-1}) |
| 1 | SDSS J094046+033930 | 145.19287 | 3.65839 | 0.08730 | 392.8 | 7.94 | 20.55 | 1.11 | 16.61 | 4.86 | 42.94 | < 41.40 |
| 2 | SDSS J094506+035551 | 146.27664 | 3.93087 | 0.15593 | 733.6 | 7.68 | 11.93 | 0.51 | 4.68 | 1.20 | 42.73 | < 42.39 |
| 3 | SDSS J100328+554154 | 150.86636 | 55.69831 | 0.14602 | 682.8 | 7.53 | 13.89 | 0.82 | 4.72 | 1.22 | 42.39 | < 42.36 |
| 4 | SDSS J101757+390528 | 154.48708 | 39.09110 | 0.05392 | 237.0 | 7.29 | 4.59 | 0.55 | 4.94 | 1.35 | 41.33 | < 41.19 |
| 5 | SDSS J102142+130550 | 155.42455 | 13.09733 | 0.07650 | 341.7 | 6.93 | 4.32 | 0.68 | 9.69 | 3.30 | 41.83 | < 41.23 |
| 6 | SDSS J111521+424217 | 168.83784 | 42.70484 | 0.19714 | 950.9 | - | > 33.63 | 0.57 | > 33.30 | > 6.88 | 44.68 | < 42.15 |
| 7 | SDSS J115658+550822 | 179.24117 | 55.13932 | 0.07980 | 357.2 | 7.72 | 17.04 | 1.10 | 7.40 | 2.52 | 42.96 | < 41.62 |
| 8 | SDSS J121355+024753 | 183.47861 | 2.79806 | 0.07429 | 331.3 | 6.77 | 6.44 | 0.62 | 6.30 | 2.05 | 42.49 | < 41.23 |
| 9 | SDSS J123026+414258 | 187.60876 | 41.71606 | 0.12486 | 576.0 | 7.50 | 8.82 | 0.70 | 8.53 | 2.93 | 42.58 | < 41.77 |
| 10 | SDSS J134133-002432 | 205.38905 | -0.40892 | 0.07173 | 319.3 | < 8.30 | 11.66 | 0.62 | 6.34 | 2.07 | 42.07 | < 41.60 |
| 11 | SDSS J135858+651546 | 209.61739 | 65.26288 | 0.03259 | 141.1 | 6.85 | 3.48 | 0.77 | 9.78 | 3.32 | 41.48 | < 40.96 |
| 12 | SDSS J142931+425149 | 217.37810 | 42.86364 | 0.15500 | 728.8 | 7.60 | 9.14 | 0.79 | 12.09 | 3.94 | 42.32 | < 42.16 |
| 13 | SDSS J215650-074533 | 329.20630 | -7.75905 | 0.05541 | 243.8 | 7.14 | 9.43 | 0.43 | 4.41 | 1.02 | 41.61 | < 41.49 |
| 14 | SDSS J221742+000908 | 334.42340 | 0.15209 | 0.04514 | 197.2 | 6.36 | 14.53 | 1.85 | 11.15 | 3.71 | 41.80 | < 40.56 |

NOTES: (1) Source-identification; (2) SDSS source name; (3–4) J2000 positional co-ordinates from the SDSS-DR7; (5) SDSS spectroscopic redshift; (6) luminosity distance in megaparsecs calculated using our adopted cosmology; (7) logarithm of black hole mass in units of solar masses derived from the stellar velocity dispersion (MPA-JHU DR7 release) using the M - σ relation (Gebhardt et al. 2000); (8–10) Emission-line ratios from SDSS-DR7; (11) Implied A_V in magnitudes derived from the Balmer decrement ($H\alpha/H\beta$; see section 2.1.3); (12) Logarithm of dust extinction corrected [OIII] luminosity; (13) Logarithm of the 3σ upper limit of the 2–10 keV X-ray luminosity derived from fluxes produced using FLIX (see footnote 4).

Netzer et al. 2006; Panessa et al. 2006). In order to identify obscured AGN candidates, we follow Maiolino et al. (1998) and Bassani et al. (1999) by using the flux ratio of de-reddened (intrinsic) [OIII] and observed (absorbed) 2–10 keV X-ray emission, and compare it to the [OIII]/ $H\beta$ ratio in a new diagnostic diagram analogous to a BPT diagram; see Fig. 2. Optical luminosities are corrected for dust-reddening towards the AGN NL-region using the Balmer decrement (i.e., the observed $H\alpha$ - $H\beta$ ratio; Ward et al. 1987), an intrinsic ratio of 3.1 (Osterbrock & Ferland 2006) and a standard $R = 3.1$ Cardelli et al. (1989) extinction curve. The parent AGN sample are found to have de-reddened [OIII] luminosities in the range $L_{[\text{OIII}]} \approx (0.03\text{--}500) \times 10^{42} \text{ erg s}^{-1}$ (median $L_{[\text{OIII}]} \approx 10^{42} \text{ erg s}^{-1}$). AG09 find that the average X-ray-[OIII] flux ratio for unobscured AGNs (i.e., Type 1s; $N_H < 10^{22} \text{ cm}^{-2}$) is ≈ 30 , whilst heavily obscured AGNs (Type 2s) typically exhibit lower values of $f_X/f_{[\text{OIII}]}$. AGNs with $f_X/f_{[\text{OIII}]} < 0.1$ are invariably found to be Compton thick and a significant proportion of Compton-thick AGNs have $f_X/f_{[\text{OIII}]} \sim 0.1\text{--}1.0$ in addition to heavily absorbed Compton-thin AGNs. One-hundred and forty-seven (≈ 63 percent) of the 233 X-ray undetected AGNs have $f_X/f_{[\text{OIII}]} < 1.0$ (24 have $f_X/f_{[\text{OIII}]} < 0.1$) from which we select a representative sub-sample of 14 (≈ 10 percent) to be further investigated using pointed mid-IR spectroscopic and photometric observations. Our sample of 14 AGNs are well-matched to the parent sample of X-ray undetected AGNs with a redshift distribution of 0.03–0.2 (median ~ 0.08) and $L_{[\text{OIII}]} \approx (0.2\text{--}500) \times 10^{42} \text{ erg s}^{-1}$ (median $L_{[\text{OIII}]} \approx 2 \times 10^{42} \text{ erg s}^{-1}$). For completeness, we also note that 11/14 of our sources are detected in at least one of the softer X-ray bands ($E < 2 \text{ keV}$) in 2XMMi. These detections, in many cases, may be due to a scattered or reprocessed soft X-ray component (e.g., Matt et al. 2000).

Clearly, this softer component may partially contribute to the flux at $E > 2 \text{ keV}$. However, any correction which could be made to our 3σ upper-limits would only serve to reduce the current hard-band limits. The basic source properties for our sample of 14 candidate Compton-thick AGNs are shown in Table 1.

3 MID-IR SPECTROSCOPY AND PHOTOMETRY

We have used the *Spitzer* Infra-Red Spectrograph (IRS) and Multi-band Imaging Photometry for *Spitzer* (MIPS) to observe the 14 candidate Compton-thick AGNs selected in Section 2 (PID:50818; PI: D.Alexander). In this section, we present the reduction methodology and resulting spectroscopy and photometry for these 14 targets. In order to robustly assess the intrinsic luminosity of the central sources in these AGNs, we also present mid-IR spectral decomposition analyses to isolate the AGN continuum and star-formation emission.

3.1 *Spitzer*-IRS Spectral Reduction and Analysis

Each of the 14 candidate Compton-thick AGNs were observed in spectral staring mode with the low-resolution modules (short-low [SL; 5.2–14.5 μm] and long-low [LL; 14.0–38.0 μm]; $R \approx 57\text{--}127$) of the *Spitzer*-IRS instrument (Houck et al. 2004). The sources were observed between 30th November 2008 and 24th February 2009 using ramp durations of 60 seconds \times 10 (4) cycles and 120 seconds \times 4 cycles for the SL1 (SL2) and LL modules, respectively. The total integration time for each of the sources was 0.5 hours.

The two-dimensional Basic Calibrated Data (BCDs)

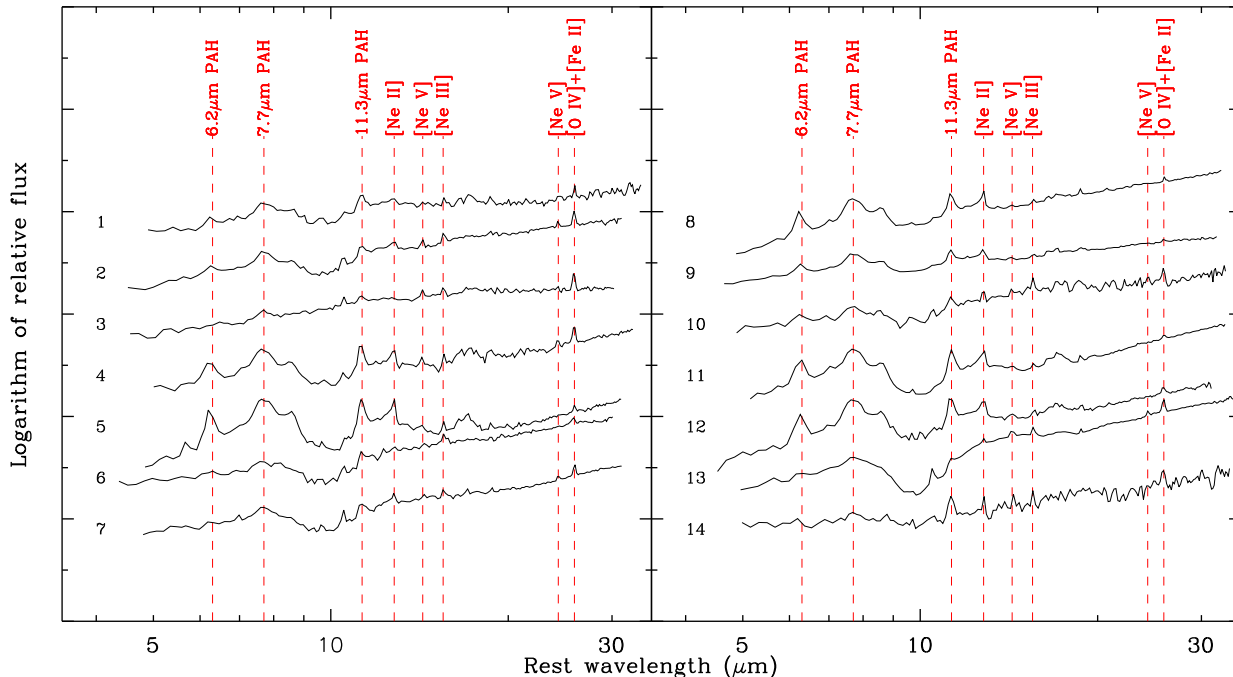


Figure 3. Rest-frame low-resolution *Spitzer*-IRS spectroscopy of the 14 X-ray undetected SDSS AGNs in our sample. The prominent emission-line and PAH features that may be detected are highlighted.

images produced by the S18.7.0 *Spitzer* Science Center (SSC) pipeline were retrieved and further analyzed using our custom IDL reduction routine (see Goulding 2010). Individual BCDs were rigorously cleaned of rogue ‘hot’ pixels using a customised version of IRSCLEAN. Next, individual rows were fit as a function of time to remove latent charge which exists on the detector after bright and/or long observations. The cleaned BCDs were averaged in the differing nod positions, which were then used to perform alternate background subtractions of the source in each nod position.

Spectral extraction was performed using the *Spitzer*-IRS Custom Extraction (SPICE) software provided by the SSC. The spectroscopy was extracted using an optimally calibrated 2-pixel wide spectral window to maximize the signal-to-noise ratio of each spectrum. Flux uncertainties were estimated for each of the spectra using a second spectral window offset from the source in the spatial direction. The spectra for each of the modules for an individual object were corrected for their differing apertures and normalized to the flux level of the 1st LL module. Orders were clipped of spectral noise (see the *Spitzer*-IRS handbook for further information) and stitched together by fitting low-order polynomials to produce the final spectra.

3.2 *Spitzer*-MIPS Reduction and Analysis

In order to measure accurate emission-line and continuum fluxes we use *Spitzer*-MIPS 24 μm photometry to flux calibrate the IRS spectroscopy. Eleven of our 14 *Spitzer*-IRS targets were observed with the MIPS photometer. The remaining three sources were scheduled but were not observed before the depletion of the instrument’s cryogenic liquid coolant.

BCDs were retrieved and the data reduced using the SSC analysis program MOPEX. We post-process individual BCD frames to remove common MIPS artifacts (i.e., ‘jail-bars’, latents etc.) and suppress large and small-scale gradients using master-flat images generated from the initial data. Processed frames were then background matched, stacked, mosaicked and median filtered using MOPEX to create the final background-subtracted reduced image.

Point source extraction was performed using the SSC provided *Spitzer* Astronomical Point Source EXtraction (APEX) software to produce 24 μm aperture photometric fluxes of the sources in the reduced MIPS frames (see column 5 of Table 2). The IRS spectra were convolved with the 24 μm MIPS response curves and compared to the photometric fluxes to produce absolute flux calibrated IRS spectra of each source. The average upwards photometric correction required to the spectroscopy was a factor of ≈ 1.3 . For the three objects lacking MIPS observations (see Table 2) we did not attempt to correct these spectra. Hence, we consider the emission-line and continuum fluxes (derived in sections 3.3 and 3.4) for these three AGNs to be less accurate and most likely conservative lower-limits.

3.3 Mid-IR Emission-line Fluxes

The reduced and flux-calibrated mid-IR spectra produced in the previous sections were further analyzed (i.e., fitting of emission-lines and polycyclic aromatic hydrocarbon features) using the *Spitzer* spectral analysis program, SMART (Higdon et al. 2004). Typical AGN dominated emission lines present in the spectra of these sources included [NeV]

($\lambda\lambda 14.32, 24.32 \mu\text{m}$) and [OIV] + [FeII] ($\lambda\lambda 25.89, 25.99 \mu\text{m}$).⁵ Additionally, AGN and star-formation produced lines such as [NeII] ($\lambda 12.82 \mu\text{m}$) and [NeIII] ($\lambda 15.51 \mu\text{m}$) were also present. See Table 2 for the *Spitzer*-IRS derived properties and see Fig 3 for the final *Spitzer*-IRS spectra.

Mid-IR high-excitation narrow-line emission such as [NeV] and [OIV] (ionisation potentials of 97.1 eV and 54.9 eV, respectively) have been shown to be excellent extinction-free unambiguous indicators of the bolometric luminosity of an AGN (e.g., Meléndez et al. 2008; Diamond-Stanic et al. 2009; Goulding et al. 2010). From analysis of our *Spitzer*-IRS spectroscopy, we find that six of the AGNs in our sample have detected [NeV] emission and all 14 have detected [OIV] + [FeII].⁶ The [NeV] and [OIV] luminosities for the six AGNs with detected [NeV] are well correlated and lie within the intrinsic scatter of Equation 2 of Goulding & Alexander (2009) and the more recent calibration of Weaver et al. (2010); for the sources with [NeV] 3σ upper-limits, we find that the majority of the fluxes are also consistent with these relationships. Hence, we confirm that the [OIV] emission in these particular sources is likely to be a good indicator of the intrinsic luminosity of the AGN. For AGNs with strong contributions from star-formation, the [FeII] emission may contaminate the measured [OIV] flux measured from low-resolution *Spitzer*-IRS spectroscopy (Meléndez et al. 2008). For those galaxies which we find to be dominated by star formation at mid-IR wavelengths (i.e., AGN contributions of < 50 percent; see Section 3.4), we conservatively apply a small downwards correction factor of ≈ 1.5 (Meléndez et al. 2008) to our measured [OIV] flux to account for the [Fe II] contamination. Our final adopted [OIV] luminosities cover the range, $L_{[\text{OIV}]} \approx (0.15\text{--}20) \times 10^{41} \text{ erg s}^{-1}$.

3.4 Spectral Decompositions

The low-resolution mid-IR spectra of typical Type-2 AGNs at rest-frame $\lambda \approx 4\text{--}15 \mu\text{m}$ are composed of three primary components: 1) a power-law like thermal AGN dust continuum; 2) a star-formation component which arises from the super-position of PAH features; and 3) a silicate absorption feature at $\lambda \approx 9.7 \mu\text{m}$ produced by the hot dust continuum being absorbed by cooler dust on parsec scales (e.g., Goulding & Alexander 2009; Gallimore et al. 2010; Mullaney et al. 2010; Tommasin et al. 2010). Therefore, as expected, we find that the mid-IR spectra for the majority of our candidate Compton-thick AGNs contain both an AGN produced continuum and strong polycyclic aromatic hydrocarbon (PAH) features, which are associated with starburst activity in the circumnuclear photodissociation regions of the host galaxy. Here we outline our spectral decomposition routine to determine the relative contributions of starburst (SB) activity and the AGN continuum in our 14 Compton-thick AGN candidates (i.e., the SB:AGN ratio), and measure the intrinsic luminosity of the central source from the AGN produced mid-IR continuum at $6 \mu\text{m}$ (e.g., Lutz et al. 2004).

Using a purpose-built IDL-based routine, we fit the IRS spectroscopy for each of the 14 candidate Compton-thick AGNs with a combined standard starburst template and an AGN power-law component (with spectral index, k) convolved with a Draine & Li (2007) extinction curve ($\rho(\lambda)$) of the form,

$$f_{AGN}(\lambda) = a\lambda^k \exp[-b\tau\rho(\lambda)] \quad (1)$$

where a , b and k are constants, and τ is the optical depth.⁷ Within the fitting we use four possible starburst templates which cover a realistic range of physical and theoretical scenarios: 1) low-resolution *Spitzer*-IRS spectroscopy of the archetypal starburst galaxy, M82; 2) a combined *Spitzer*-IRS starburst template of local pure star-forming galaxies presented in Brandl et al. (2006);⁸ 3) a theoretical radiative transfer model of a pure circumnuclear starburst region at $r \approx 3 \text{ kpc}$ with $L_{\text{IR}} \approx 10^{10} L_{\odot}$ (Siebenmorgen & Krügel 2007; hereafter, SK07); and 4) a theoretical radiative transfer model of a nuclear star cluster at $r < 0.35 \text{ kpc}$ with $L_{\text{IR}} \approx 10^{10} L_{\odot}$ (SK07).

The best resulting model parameters derived from the minimum Chi-squared fit to the IRS data are given in Table 2 and shown in Fig. 4. We note that none of the AGNs in our sample have mid-IR spectral features which are consistent with the theoretical nuclear star cluster model, and hence, the best-fit spectral model for each are that of an AGN combined with one of the three circumnuclear starburst templates. Based on the mid-IR spectral-fits, we also derive the approximate contribution of the AGN to the mid-IR emission for each of the sources; see column (7) of Table 2. We find that although these AGNs were selected to be strong [OIII] and [NII] emitters (i.e., optically-dominated Seyfert galaxies), the mid-IR spectra of ≈ 50 percent of the sources are consistent with being dominated by star-formation activity. Indeed, on the basis of these spectral decompositions, the mid-IR spectroscopy for one source (SDSS J102142+130550) is consistent with there being no AGN component, despite this source clearly being identified as an AGN at optical wavelengths.

In order to estimate the intrinsic AGN luminosity and hence place limits on the X-ray absorption in these sources, we use the measured AGN power-law parameters to derive $6 \mu\text{m}$ luminosities ($L_{6\mu\text{m}}$). The uncertainties of these $6 \mu\text{m}$ fluxes are established by considering a weighted spread in the measured $6 \mu\text{m}$ fluxes from all statistically valid starburst template fits (i.e., we reject all statistically poor fits at the 95 per cent level). The mean 1σ uncertainty is ≈ 0.1 dex. See column (8) of Table 2.

We estimate the $6 \mu\text{m}$ continuum luminosities for 13 of our 14 candidate Compton-thick AGNs and conservatively estimate an upper limit for the $6 \mu\text{m}$ continuum flux of $< 10^{-2} \text{ mJy}$ for SDSS J102142+130550. We find using our adopted cosmology, that the AGNs cover more

⁵ We note that due to the spectral resolution of the LL modules, the [OIV] and [FeII] emission lines cannot be individually resolved.

⁶ We note that the identification of some AGNs even in the very nearby Universe can often require extremely high signal-to-noise, high-resolution mid-IR spectroscopy (e.g., Satyapal et al. 2008; Goulding & Alexander 2009).

⁷ Our IDL routine is based on that used by Mullaney et al. (2010b) and makes use of the Markwardt 1-dimensional Chi-squared analysis library, see <http://cow.physics.wisc.edu/~craigm/idl/> for further details.

⁸ We note that as we require only starburst emission in these templates, we do not include galaxies in the combined Brandl starburst template which have any previous evidence for AGN activity (i.e., Mrk 266, NGC 660, 1097, 1365, 3628 and 4945).

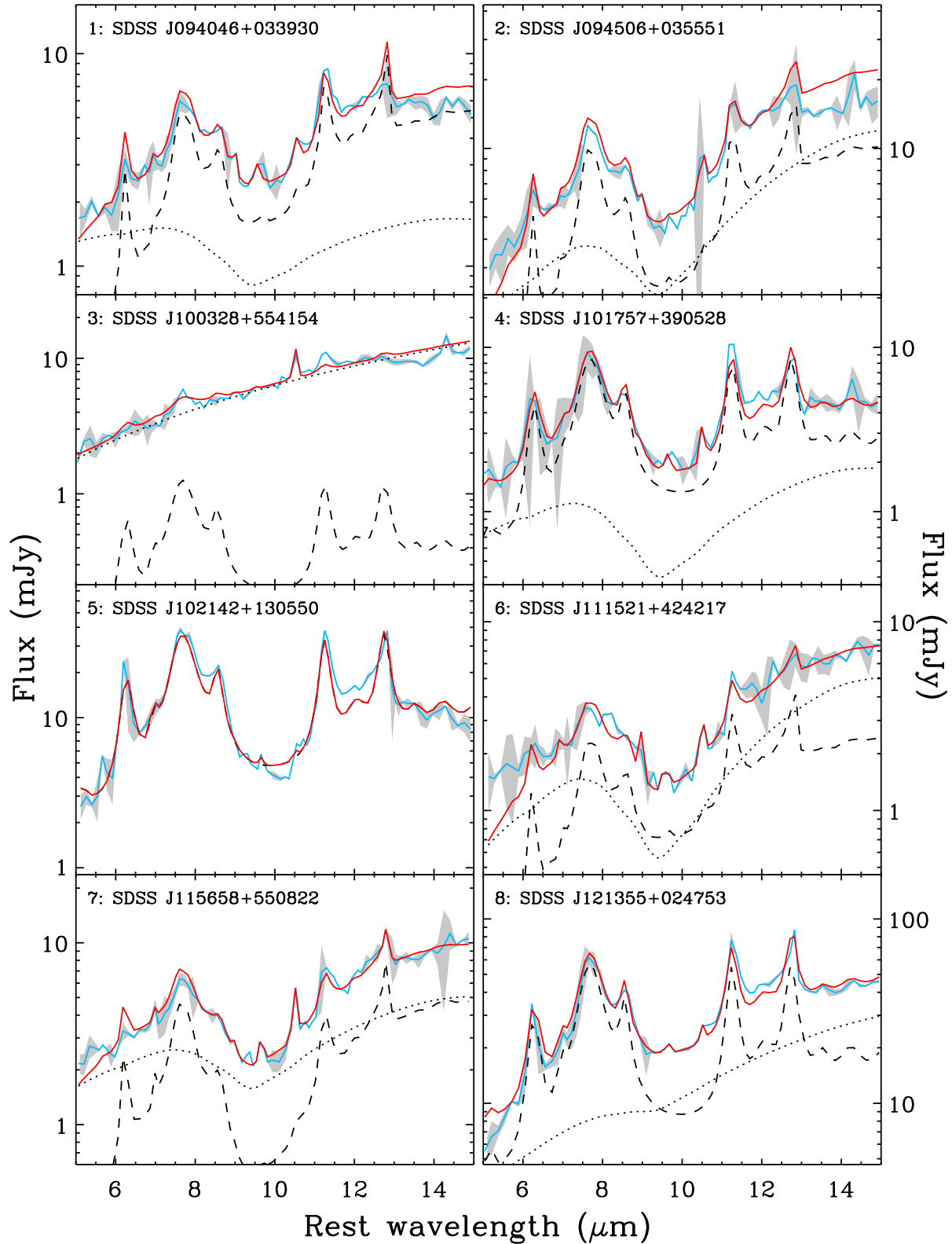


Figure 4. Spectral decompositions of the *Spitzer*-IRS spectra (blue solid curve) for our candidate Compton-thick AGNs produced by our spectral analysis program as described in section 3.4. The grey shaded region indicates the 1σ flux uncertainties to the observed spectrum. The best-fit absorbed power-law and starburst template are shown with dotted and dashed curves, respectively. See Table 2 for best-fitting parameters. The total best-fit spectrum (i.e., power-law+starburst+emission-lines) is shown with a solid red curves.

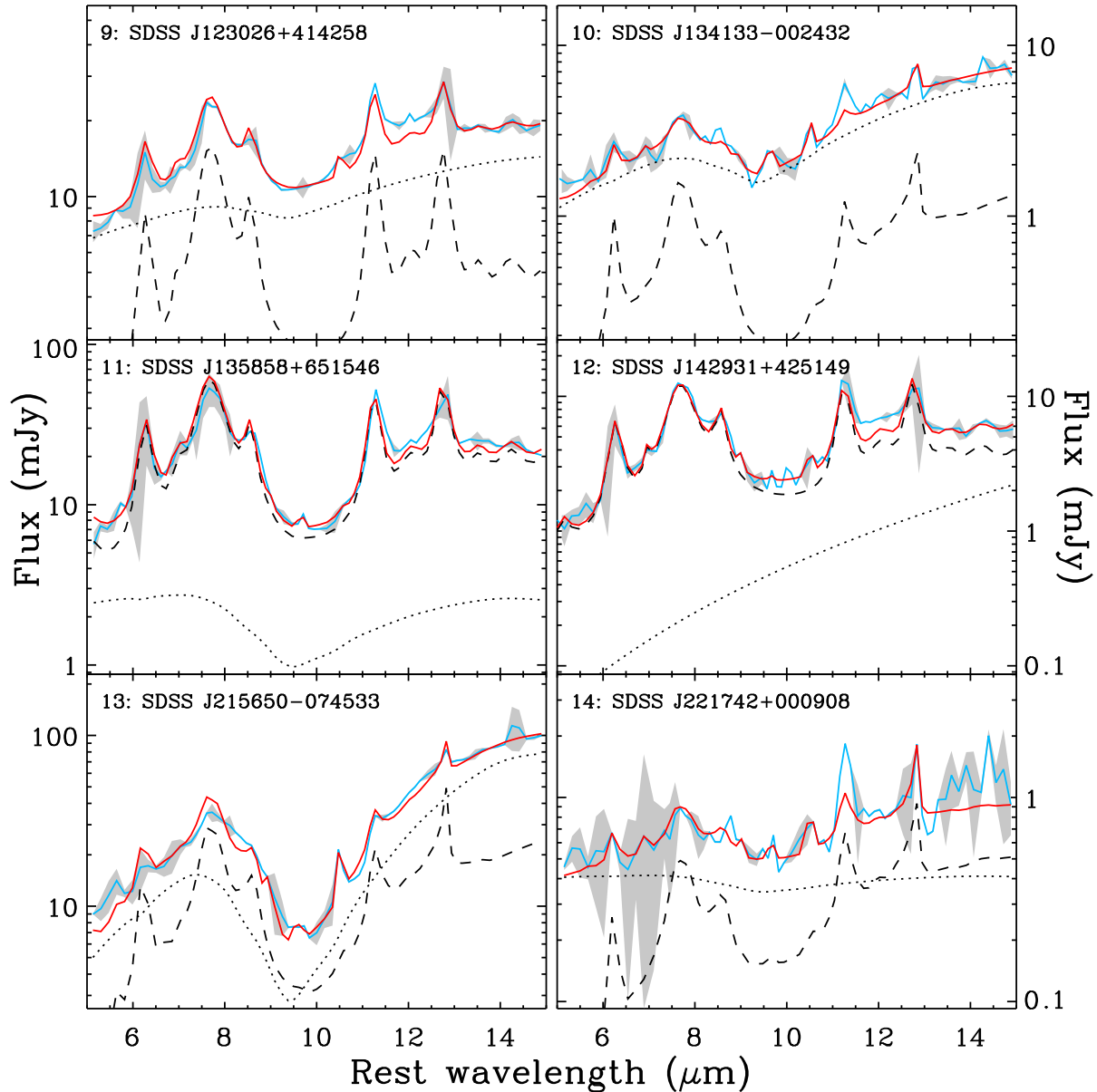


Figure 4 – continued

than 2 decades in $6 \mu\text{m}$ luminosity, with $\nu L_{6\mu\text{m}} \approx (0.1\text{--}20) \times 10^{43} \text{ erg s}^{-1}$.

4 RESULTS AND DISCUSSION

We have selected a sample of 14 [OIII] bright, X-ray undetected AGNs from the $\approx 100 \text{ deg}^2$ overlap region between the SDSS-DR7 and 2XMMi surveys. These sources lie at $z \sim 0.03\text{--}0.2$ and host moderate to highly luminous AGNs with de-reddened $L_{[\text{OIII}]}$ $\approx (0.2\text{--}500) \times 10^{42} \text{ erg s}^{-1}$ (i.e., similar to those of typical nearby Seyfert galaxies). Our 14 targets all have $f_X/f_{[\text{OIII}]} < 1$, implying strong intrinsic absorption of their X-ray flux and many (possibly all) are likely Compton-thick AGNs. In the absence of X-ray spectroscopic data, in section 3 we derived AGN-produced

emission line and continuum luminosity measurements in order to independently constrain the intrinsic luminosity of these candidate Compton-thick AGNs. In this section, we use these intrinsic luminosities in conjunction with X-ray constraints from *XMM-Newton* data to test whether these objects are indeed Compton-thick AGNs. We then use these results to place new constraints on the space density and relative mass-accretion rates of Compton-thick AGNs in the nearby Universe ($z \sim 0.1$).

4.1 Identifying Compton-thick AGNs at $z \sim 0.1$

Previously, strong, relatively high-excitation emission lines, such as [OIII] $\lambda 5007$ (35.1 eV), have been used as proxies for hard X-ray emission in AGNs, and hence,

Table 2. Measured AGN properties

| ID | [NeV] $\lambda 14.32$ | [NeV] $\lambda 24.32$ | [OIV] $\lambda 25.89$ | $S_{24\mu\text{m}}$ | SB | AGN | $S_{6\mu\text{m}}$ | $\log(L_{X,[OIV]})$ | $\log(L_{X,6\mu\text{m}})$ | $\log(\eta)$ | C-thick? | |
|-----|--|--|--|---------------------|-------|--------|--------------------|-------------------------|----------------------------|--------------|-----------------------|------|
| (1) | (2) | (3) | (4) | (5) | (6) | (7) | (8) | (9) | (10) | (11) | (12) | (13) |
| | ($\text{erg s}^{-1} \text{cm}^{-2}$) | ($\text{erg s}^{-1} \text{cm}^{-2}$) | ($\text{erg s}^{-1} \text{cm}^{-2}$) | (mJy) | Model | cont. | (mJy) | (erg s^{-1}) | (erg s^{-1}) | | [OIV] $6 \mu\text{m}$ | |
| 1 | < 0.98 | < 0.77 | 3.91 ± 0.81 | 3.98 ± 0.04 | 2 | 40% | 1.71 ± 0.14 | 42.67 | 42.74 | -2.24 | y | y |
| 2 | 10.51 ± 1.43 | 6.60 ± 2.09 | 29.39 ± 1.05 | 17.82 ± 0.05 | 2 | 55% | 3.27 ± 0.19 | 44.42 | 43.58 | -0.94 | Y | y |
| 3 | 4.07 ± 0.78 | 4.07 ± 0.78 | 6.45 ± 2.03 | 8.49 ± 0.03 | 3 | 92% | 2.49 ± 0.02 | 43.63 | 43.30 | -1.02 | y | ? |
| 4 | 3.58 ± 0.55 | 3.65 ± 0.54 | 12.89 ± 0.64 | - | 3 | 38% | 1.30 ± 0.76 | 42.76 | 42.08 | -2.28 | Y | ? |
| 5 | < 2.94 | < 1.00 | 6.79 ± 1.62 | 8.90 ± 0.05 | 3 | < 0.1% | < 0.01 | 42.80 | - | - | Y | - |
| 6 | < 1.67 | < 0.78 | 5.64 ± 0.91 | 6.80 ± 0.03 | 2 | 72% | 1.42 ± 0.17 | 43.88 | 43.34 | - | Y | y |
| 7 | 3.33 ± 0.98 | 2.95 ± 0.95 | 10.90 ± 1.38 | 10.72 ± 0.10 | 2 | 53% | 2.53 ± 0.31 | 43.26 | 42.74 | -1.92 | Y | y |
| 8 | 7.40 ± 1.81 | < 2.19 | 19.07 ± 1.03 | 65.36 ± 0.06 | 3 | 38% | 5.47 ± 0.99 | 43.26 | 43.01 | -0.63 | Y | Y |
| 9 | < 2.07 | < 1.47 | 5.24 ± 0.90 | - | 3 | 66% | 8.36 ± 0.33 | 43.45 | 43.69 | -0.50 | Y | Y |
| 10 | < 1.08 | < 1.32 | 6.52 ± 0.92 | 6.93 ± 0.04 | 1 | 85% | 1.95 ± 0.11 | 42.91 | 42.52 | -2.75 | y | ? |
| 11 | < 2.46 | < 3.39 | 12.89 ± 1.92 | 39.94 ± 0.03 | 3 | 12% | 3.47 ± 2.71 | 42.26 | 42.06 | -1.87 | y | y |
| 12 | < 1.07 | < 0.63 | 4.68 ± 0.76 | 6.33 ± 0.03 | 3 | 9% | 0.09 ± 0.40 | 43.35 | 41.91 | -2.79 | ? | ? |
| 13 | 57.16 ± 3.16 | 42.17 ± 6.52 | 180.77 ± 6.01 | 106.90 ± 0.55 | 1 | 81% | 16.42 ± 3.20 | 44.24 | 43.23 | -0.73 | Y | Y |
| 14 | < 1.44 | < 0.96 | 3.06 ± 0.51 | - | 2 | 62% | 0.43 ± 0.09 | 42.09 | 41.44 | -2.10 | Y | ? |

NOTES: (1) SDSS source-identification. (2-4) Fluxes and their 1σ uncertainty for the measured AGN-produced mid-IR emission lines in units of $10^{-15} \text{ erg s}^{-1} \text{ cm}^{-2}$. (5) MIPS 24 μm flux density in units of mJy. (6) Best-fit starburst model in the mid-IR spectral modeling analysis (see section 3.4) - 1: M82; 2: Combined SB (Brandl et al. 2006); 3: Circumnuclear starburst at 3 kpc (SK07). (7) Inferred AGN contribution to the mid-IR emission at $\lambda \sim 5\text{--}15 \mu\text{m}$. (8) Unabsorbed AGN 6 μm flux and 1σ uncertainty in units of mJy. (9-10) Logarithm of the estimated 2–10 keV luminosity from the AGN-produced [OIV] and 6 μm emission (see sections 3.3, 3.4 and 4.1 for further details). (11) Logarithm of implied Eddington ratio derived from the estimated 2–10 keV luminosity using 6 μm emission, and the SMBH masses presented in Table 1. (12-13) Indication for whether the source is consistent with being Compton-thick ($N_H > 1.5 \times 10^{24} \text{ cm}^{-2}$) on the basis of the mid-IR indicators: ‘Y’ - conservatively identified to be Compton-thick, ‘y’ - less-conservatively identified to be Compton-thick, ‘?’ - inconclusive due to depth of current X-ray data (i.e., they are upper-limits; see section 4.1).

their intrinsic luminosity (L_{AGN} ; e.g., Mulchaey et al. 1994; Alonso-Herrero et al. 1997; Heckman et al. 2005; Panessa et al. 2006). However, such emission may also be readily excited by strong star formation as well as being subject to significant dust extinction within the host galaxy. By contrast, mid-IR high-excitation narrow-line emission (e.g., [NeV]; [OIV]) is an excellent extinction-free indicator of L_{AGN} (see Section 3.3) and, when combined with sensitive X-ray data, can provide good first order constraints on whether an AGN is Compton thick.

In Fig. 5a we present the observed 2–10 keV X-ray upper-limit luminosities from the *XMM-Newton* data versus the mid-IR [OIV] luminosity for our candidate Compton-thick AGNs and compare them to the intrinsic properties found for local ‘bona-fide’ Compton-thick AGNs. We find that the candidate Compton-thick AGNs are spread over a wide range of [OIV] luminosities, $L_{[\text{OIV}]} \approx (0.13\text{--}20) \times 10^{41} \text{ erg s}^{-1}$; for the sources in our sample which we find to be dominated by SF at mid-IR wavelengths (column 7 of Table 2), [OIV] fluxes have conservatively been adjusted for contamination from [FeII] emission (see section 3.3). We find that based on the observed X-ray upper-limits, none of the objects in our sample are consistent with the local intrinsic relation of AGNs from Goulding et al. (2010), suggesting that the X-ray emission is heavily obscured. However, as we illustrate in Fig. 5a, the observed $L_X/L_{[\text{OIV}]}$ for our sample (mean ratio ≈ 3.6) is consistent with the observed $L_X/L_{[\text{OIV}]}$ ratio for a sample of well-studied local ‘bona-fide’ Compton-thick AGNs (i.e., Circinus, Mrk 3, NGC 1068 and NGC 6240). Furthermore, the $L_X/L_{[\text{OIV}]}$

luminosity ratio of these four Compton-thick AGNs is consistent with the $L_X\text{--}L_{[\text{OIV}]}$ relationship of Goulding et al. (2010) when the X-ray data is corrected for the absorption implied from high-quality X-ray spectroscopy. Assuming the [OIV] emission is indeed an isotropic AGN indicator (e.g., Melendez et al. 2008; Diamond-Stanic et al. 2009; Goulding et al. 2010), this suggests that by comparing the observed X-ray upper-limit to the intrinsic X-ray luminosity as predicted by our [OIV] measurements ($L_{X,[\text{OIV}]}$), we may infer whether the sources in our sample are indeed Compton-thick AGNs.

Based on Compton reflection models, Alexander et al. (2008) predict that the observed–intrinsic X-ray flux ratio in the 2–10 keV band for a Compton-thick AGN with $N_H \sim 1.5 \times 10^{24} \text{ cm}^{-2}$ is $f_{X,\text{intr}}/f_{X,\text{obs}} \approx 15$. Hence, we predict that sources with $f_{X,\text{intr}}/f_{X,\text{obs}} \gtrsim 15$ are likely to be obscured by Compton-thick material. For the 14 candidate Compton-thick AGNs in our sample, we calculate $f_{X,[\text{OIV}]}$ using the local X-ray–[OIV] relation of Goulding et al. (2010). We predict intrinsic X-ray luminosities of $L_{X,\text{predict}} \approx (0.1\text{--}26) \times 10^{43} \text{ erg s}^{-1}$ (see Column 9 of Table 2). We find that 13 (≈ 90 percent) of the sources exhibit $f_{X,[\text{OIV}]} / f_{X,\text{obs}} \gtrsim 15$ (see Column 12 of Table 2). Furthermore, if we account for the intrinsic scatter within the local relation (≈ 0.3 dex), and conservatively assume that none of the sources which lie within this region are Compton-thick, we still estimate that at least 9/14 (≈ 65 percent) of our candidate Compton-thick AGNs could be genuine Compton-thick AGNs. It is also prudent to note that as the observed X-ray fluxes for all of these sources are upper-limits, we cannot exclude the

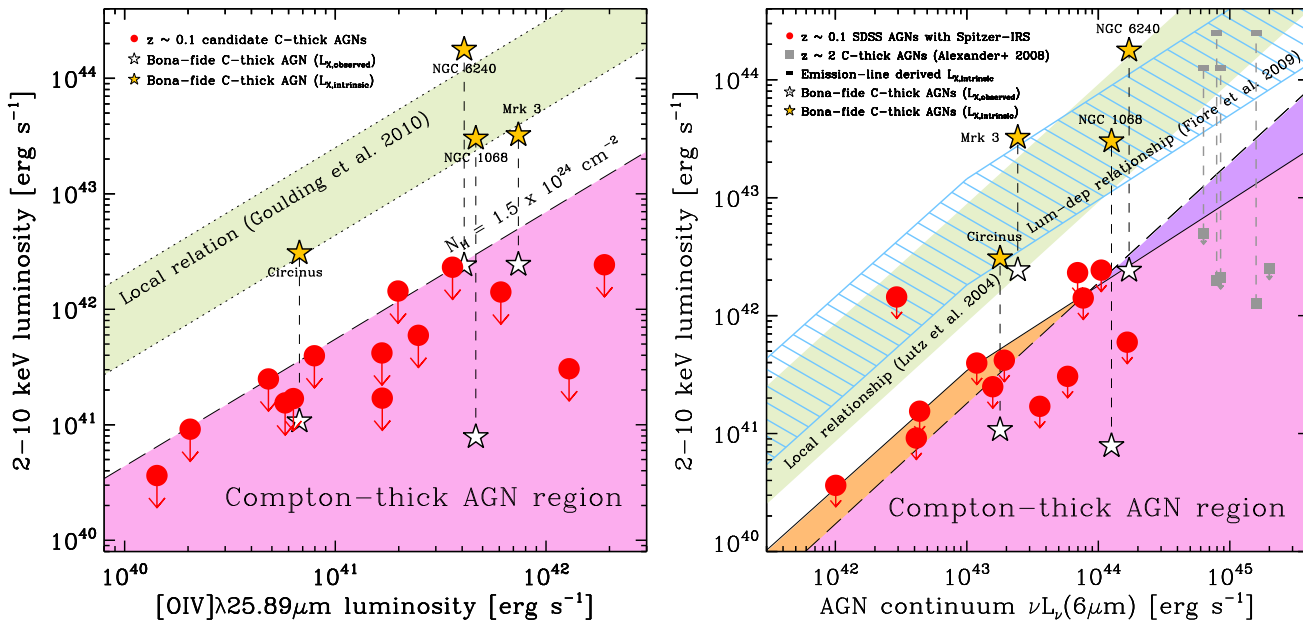


Figure 5. **Left; (a):** Rest-frame 2–10 keV X-ray luminosity versus mid-IR [OIV] ($\lambda 25.89 \mu\text{m}$) luminosity ($L_{[\text{OIV}]}$) for our sample of Compton-thick AGN candidates (filled circles). We show the local X-ray–[OIV] relation of Goulding et al. (2010) and find on the basis of $L_{[\text{OIV}]}$ that the majority of our sample are consistent with the observed X-ray luminosity being absorbed by a factor ≥ 15 (i.e., $N_H > 1.5 \times 10^{24} \text{ cm}^{-2}$). **Right (b):** Rest-frame 2–10 keV X-ray luminosity versus the mid-IR AGN continuum luminosity at $6 \mu\text{m}$ for the Compton-thick AGN candidates with measured $6 \mu\text{m}$ luminosities (filled circles). A comparison sample of $z \sim 2$ Compton-thick quasars is additionally shown (Alexander et al. 2008; grey squares). We use the local X-ray– $6 \mu\text{m}$ relation of Lutz et al. (2004) and the luminosity-dependent relation of Fiore et al. (2009) to predict the region of parameter space where Compton-thick AGN lie. We find that on the basis of $6 \mu\text{m}$ luminosities, many of the sources in our sample are likely to be Compton-thick AGNs. For comparison, in both (a) and (b) we additionally highlight the observed (filled stars) and absorption-corrected (open stars) X-ray luminosities for 4 well-studied ‘bona-fide’ Compton-thick AGNs (Circinus, Mrk 3, NGC 1068 and 6240). In both figures, the observed X-ray luminosities for these ‘bona-fide’ Compton-thick AGNs occupy roughly the same region of parameter space as our sample but our objects are ≈ 10 – 100 times more distant. However, their intrinsic X-ray luminosities are consistent with the local relations.

possibility that all of the sources in our sample are Compton-thick AGNs as the implied $f_{X,[\text{OIV}]} / f_{X,\text{obs}}$ ratio is a lower-limit.

By combining multiple indirect AGN luminosity indicators, particularly those which probe different regions of the central engine, we can place even stronger constraints on whether the AGNs in our sample are Compton thick than using narrow-line emission alone. The $6 \mu\text{m}$ continuum luminosity has been shown to provide a good proxy for the intrinsic AGN luminosity (e.g., Lutz et al. 2004; Maiolino et al. 2007; Treister et al. 2008; Fiore et al. 2009). In Fig. 5b we again present the observed 2–10 keV X-ray upper-limit luminosities from *XMM-Newton* data but now compare these luminosities to the AGN continuum luminosity at $6 \mu\text{m}$ derived in Section 3.4 and the luminosity-dependent (Fiore et al. 2009) and luminosity-independent (Lutz et al. 2004) relations derived using high-quality X-ray data and mid-IR *Spitzer* IRAC photometry and ISO spectroscopy, respectively. As noted in Section 3.4, one of our 14 candidate Compton-thick AGNs is consistent with there being little or no mid-IR emission from an AGN continuum at $\lambda \sim 5$ – $15 \mu\text{m}$, and we remove this AGN from further analyses in here.

We conservatively adopt the slightly lower-luminosity X-ray– $6 \mu\text{m}$ relationship of Lutz et al (2004) to infer the

intrinsic X-ray luminosities of the candidate Compton-thick AGNs. We estimate intrinsic X-ray luminosities of $L_{X,\text{predict}} \approx (0.2\text{--}30) \times 10^{42} \text{ erg s}^{-1}$ (see Column 10 of Table 2). Eight out of the 13 (≈ 60 percent) $6 \mu\text{m}$ detected sample members lie in the region expected for Compton-thick AGNs (i.e., $N_H \gtrsim 1.5 \times 10^{24} \text{ cm}^{-2}$; see Column 13 of Table 2). However, if we were to adopt the relationship of Fiore et al. (2009) this Compton-thick AGN fraction would increase to 9/13 sources (≈ 80 percent; i.e., consistent with that found when using [OIV] as a N_H diagnostic). Furthermore, if we account for the intrinsic scatter of within the Lutz et al (2004) relationship (≈ 0.5 dex), and (as above) conservatively assume that none of the sources which lie within this region of scatter are genuine Compton-thick AGNs, we still find that at least 3 of the 13 (≈ 20 percent) sources must be Compton thick.

In Columns 12 and 13 of Table 2 we summarise whether we identify the sources to be Compton-thick AGNs on the basis of their combined X-ray and mid-IR properties. We consider those AGNs which are conservatively identified as Compton-thick AGNs (i.e., those which lie below the region of intrinsic scatter derived from the L_X – $L_{[\text{OIV}]}$ and L_X – $L_{6\mu\text{m}}$ relationships) in at least one of the mid-IR diagnostics and are also below the standard Compton thick threshold in the other mid-IR diagnostic to be genuine Compton-thick

AGNs (i.e., in the nomenclature of Table 2, only those AGNs with Y-Y, Y-y or y-Y). This is a reasonable and conservative assumption to make if we consider the ‘bona-fide’ Compton-thick AGNs shown in Fig. 5; all of these AGNs would be identified to be Compton-thick AGNs (y/Y) on the basis of [OIV] emission and 3/4 on the basis of 6 μm emission. Hence, using our adopted definition, we find that 6/14 (≈ 43 percent) of our candidate Compton-thick AGNs are very likely genuine Compton-thick AGNs on the basis of their combined mid-IR properties. Under the reasonable assumption that our sample of candidate Compton-thick AGNs is a representative sub-sample of the parent X-ray undetected population of AGNs in the SDSS-DR7 (i.e., in both redshift and luminosity parameter space; see section 2), these results imply that at least $\approx 43 \pm 21$ percent of the sources with $f_X/f_{\text{[OIII]}} < 1$ are Compton thick.⁹ We note that on the basis of our most conservative and most optimistic Compton-thick diagnostic thresholds, ≈ 20 –100 percent of AGNs with $f_X/f_{\text{[OIII]}} < 1$ could be Compton thick.

Of the four AGNs which were selected because they lie in the exclusively Compton-thick AGN region of Fig. 2 (i.e., those with $f_X/f_{\text{[OIII]}} < 0.1$), three have mid-IR emission-line and continuum AGN indicators consistent with the X-ray emission being absorbed by at least a factor $\gtrsim 15$. Hence, these are very likely to be Compton-thick AGNs. Whilst the [OIV] emission from the fourth AGN (SDSS J221742+000908) is consistent with a Compton-thick AGN (see Fig. 5a) we find little evidence for this on the basis of its 6 μm continuum luminosity. Indeed, the observed $L_{X,2-10\text{keV}}$ appears to be comparatively unabsorbed on the basis of AGN continuum luminosity. However, we note that we would also find a similar result for the ‘bona-fide’ Compton-thick AGN, Mrk 3. We find that five of the 10 AGNs with $f_X/f_{\text{[OIII]}} \sim 0.1$ –1.0 exhibit mid-IR emission features consistent with Compton-thick AGNs. All five AGNs have strong [OIV] and 6 μm luminosities suggesting strong absorption of the X-ray emission, as well as evidence for silicate absorption at 9.7 μm . By contrast, for the AGN which does not appear to be clearly Compton-thick on the basis of either of our mid-IR AGN indicators (SDSS J142931+425149), we find that the underlying AGN continuum in this sources is consistent with an unabsorbed power-law (i.e., no evidence for silicate absorption).

4.2 The space-density of Compton-thick AGNs at $z \sim 0.1$

Based on the mid-IR emission-line and continuum emission diagnostics, we find that at least six ($\gtrsim 43 \pm 21$ percent) of our sample of 14 X-ray undetected optical narrow-line AGNs with $L_X/L_{\text{[OIII]}} < 1$ appear to suffer from heavy intrinsic absorption with $N_H \gtrsim 1.5 \times 10^{24} \text{ cm}^{-2}$ (i.e., they are Compton-thick AGNs). Assuming that our sample of candidate Compton-thick AGNs is representative of the parent population, we may use our derived Compton-thick AGN fraction to infer at least a lower limit for the number, and hence space density, of Compton-thick AGNs at $z \sim 0.03$ –0.2.

⁹ Uncertainties are calculated using standard Poisson counting statistics.

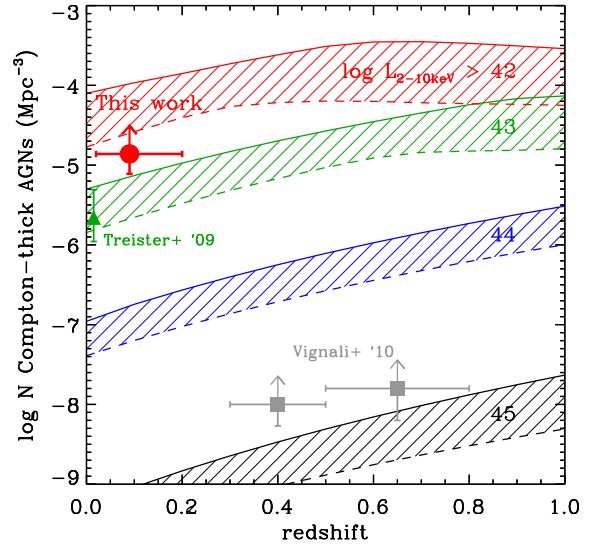


Figure 6. Space density of Compton-thick AGNs compared with the XRB synthesis models of Gilli et al. (2007; solid curves) and Treister et al. (2009; dashed curves) for intrinsic X-ray luminosities of $L_X > 10^{42}, 10^{43}, 10^{44}$ and $10^{45} \text{ erg s}^{-1}$. Data points refer to this work (solid circle; $L_X > 10^{42} \text{ erg s}^{-1}$) and those from comparable studies of $z \sim 0$ Compton-thick AGNs (Treister et al. 2009; solid triangle; $L_X > 10^{43} \text{ erg s}^{-1}$) and luminous Compton-thick quasars at $z \sim 0.3$ –0.8 derived from the SDSS (Vignali et al. 2010; solid squares; $L_X > 2.5 \times 10^{44} \text{ erg s}^{-1}$).

The total number of Type-2 AGNs in the SDSS-2XMMi overlap region is 334 at $z \sim 0.03$ –0.2, 147 (≈ 45 percent) of these AGNs are X-ray undetected in 2XMMi with $L_X/L_{\text{[OIII]}} < 1$ (i.e., our parent sample). Based on our derived Compton-thick AGN fraction above, we would expect that $\approx 63 \pm 31$ of the sources in our parent sample with $L_X/L_{\text{[OIII]}} < 1$ to be Compton-thick AGNs, i.e., ≈ 20 percent of all Type-2 AGNs in the SDSS-2XMMi overlap region. The comoving volume encompassed by our survey is $V \approx 4.6 \times 10^6 \text{ Mpc}^3$. Hence, we estimate a space-density of Compton-thick AGNs at $z \sim 0.1$ of $\log(\Phi) \approx -4.9_{-0.3}^{+0.2} \text{ Mpc}^{-3}$ for luminosities of $L_X \gtrsim 10^{42} \text{ erg s}^{-1}$. However, given that both our sample selection and method for identifying Compton-thick AGNs are based on X-ray flux upper-limits (i.e., those sources with $L_X/L_{\text{[OIII]}} > 1$ which currently lack formal X-ray detections may have $L_X/L_{\text{[OIII]}} < 1$ with deeper X-ray observations; all of the AGNs in our *Spitzer*-IRS sample may still be Compton thick), the space-density found here should be considered a strict lower-limit to the number of Compton-thick AGNs in our parent sample.

In Fig. 6 we compare our estimated space-density to the similar study of SDSS-selected Compton-thick quasars of Vignali et al. (2010) and to those derived from the XRB synthesis models of Gilli et al. (2007) and Treister et al. (2009).¹⁰ Both models invoke a large population of Compton-thick AGNs in order to fit the peak of the XRB

¹⁰ The XRB synthesis models of Gilli et al. (2007) and Treister et al. (2009) are defined using a slightly different cosmology ($H_0 = 70 \text{ km s}^{-1}$) to that considered here ($H_0 = 71 \text{ km s}^{-1}$). However,

at $E \sim 30$ keV. The differences in the required space densities of Compton-thick AGNs are derived from the normalisations to the XRB, as well as the inclusion of the local Compton-thick AGNs identified by *INTEGRAL* and *Swift* (green triangle in Fig. 6) in the model of Treister et al. (2009). We find that at the median redshift of our parent sample, our estimated space density is systematically lower than those predicted by the Gilli et al. (2007) and Treister et al. (2009) models by a factor of ≈ 8 and 2, respectively for $L_X \gtrsim 10^{42} \text{ erg s}^{-1}$. It is important to note that our estimated space density is a lower limit, and is therefore consistent with both model predictions. However, if we were to assume the highly unlikely situation that all of our parent sample of 334 AGNs are Compton thick (i.e., a predicted space density of $\log(\Phi) \approx -4.14$), this would still be systematically below the predictions of Gilli et al. (2007).

The discrepancy between our observations and the model expectations can be explained in several ways. The most obvious explanation is that our parent sample of optical SDSS NL-AGNs does not include all obscured AGNs at $0.03 < z < 0.2$. In the SDSS-DR7, only the most luminous galaxies are targeted for spectroscopic follow-up, resulting in very few ($\lesssim 10$ percent) galaxies being included in the SDSS with $M_* \lesssim 10^{10} M_\odot$ (i.e., those likely to host relatively low mass SMBHs with $M_{\text{BH}} \lesssim 10^7 M_\odot$) to $z \sim 0.1$ (e.g., Kauffmann et al. 2003). Hence, our parent sample may not include the majority of AGNs with relatively low mass SMBHs. Using our Compton-thick AGN sample we can estimate the number of low mass SMBHs not included in our derived space density. Given the L_X/M_{BH} distribution of our sample (SMBH masses for our sample are estimated from stellar velocity dispersions; see Section 4.3 for further details; see Column 7 of Table 1), $\approx (0.2\text{--}20) \times 10^{35} \text{ erg s}^{-1} M_\odot^{-1}$, at the luminosity completeness limit ($L_X \gtrsim 10^{42} \text{ erg s}^{-1}$) and assuming a similar distribution in Eddington ratios, the smallest SMBH which could conceivably be in our sample is $M_{\text{BH}} \approx 5 \times 10^5 M_\odot$; this is a factor ≈ 10 below the lowest mass Compton-thick AGN identified here ($M_{\text{BH}} \approx 5 \times 10^6 M_\odot$). We may now estimate how many Compton-thick AGNs may contain SMBHs in the mass region $M_{\text{BH}} \approx (0.5\text{--}5) \times 10^6 M_\odot$, and hence constrain the number of Compton-thick AGNs not included in our space-density estimate due to the lower mass limit of the SDSS.

If the five most conservatively identified Compton-thick AGNs with M_{BH} estimates contained SMBHs which were a factor ≈ 10 smaller in mass but had the same L_X/M_{BH} ratio, four (≈ 80 percent) would still have $L_X \gtrsim 10^{42} \text{ erg s}^{-1}$ and would therefore be included in our estimate of the space density of Compton-thick AGNs as shown in Fig. 6. Based on a simple extrapolation of the SMBH mass function of Marconi et al. (2004), AGNs hosting SMBHs with $M_{\text{BH}} \approx (0.5\text{--}5) \times 10^6 M_\odot$ are a factor ≈ 1.5 more abundant than those with $M_{\text{BH}} \approx (0.5\text{--}5) \times 10^7 M_\odot$. Hence, based on this simplistic formalism, we estimate that approximately half of all Compton-thick AGNs with $L_X \gtrsim 10^{42} \text{ erg s}^{-1}$ may contain SMBHs with $M_{\text{BH}} \approx (0.5\text{--}5) \times 10^6 M_\odot$ which are not included in our parent sample.

this has little or no effect on the conclusions drawn from the comparisons.

Obscuration and host-galaxy contamination may further prevent us from identifying all Compton-thick AGNs in our considered volume. Obscured AGNs can be misclassified when the host-galaxy over-shines the nuclear emission. In the absence of extinction, a NL-AGN with $L_X \approx 2 \times 10^{42} \text{ erg s}^{-1}$ can be almost totally diluted by a star-formation rate of $10 M_\odot \text{ yr}^{-1}$ (i.e., $\gtrsim 95$ percent of the observed $H\beta$ emission is produced in HII regions; e.g., Yan et al. 2010). The contribution of these sources to our observed space density is difficult to quantify. However, it is predicted that as many ≈ 50 percent of AGNs may show no evidence for AGN activity in their optical spectroscopy (e.g., Maiolino et al. 2003; Goulding & Alexander 2009), and would therefore not be included in our optically selected AGN sample. Allowing for the incompleteness within our optical parent sample and the possibility that many more of the AGNs studied here may be Compton thick, we suggest that our derived space density can be broadly consistent with the XRB models.

4.3 The mean growth rate of Compton-thick AGNs at $z \sim 0.1$

Some theoretical models predict that Compton-thick AGNs may harbour SMBHs which are undergoing an evolutionary phase of rapid growth (e.g., Fabian 1999; Granato et al. 2006; Hopkins et al. 2008). In this section we consider the implied Eddington ratios ($\eta \sim L_{\text{AGN}}/L_{\text{Edd}}$; where $L_{\text{Edd}} \approx 1.26 \times 10^{38} (M_{\text{BH}}/M_\odot) \text{ erg s}^{-1}$) for the Compton-thick AGNs identified in our sample with publicly available black-hole mass (M_{BH}) estimates. Stellar velocity dispersion measurements have been computed for 13 of the 14 AGNs in our sample, at least five of which we conservatively identify as Compton-thick AGNs. These measurements are publicly available in the MPA-JHU release of SDSS-DR7 and are derived from the fitting of stellar population synthesis models to the SDSS 1-D spectra.¹¹ Using the $M\text{--}\sigma$ relation of Gebhardt et al. (2000) we convert the stellar velocity dispersions to M_{BH} (see Column 7 of Table 1) in order to calculate L_{Edd} for these sources. The median SMBH mass for our sample is $M_{\text{BH}} \approx 3 \times 10^7 M_\odot$ (i.e., these AGNs host SMBHs which are similar to those identified in the optical study of Heckman et al. 2004).

In order to estimate η for our Compton-thick AGNs, we use $L_{6\mu\text{m}}$ as a proxy for L_{AGN} and we assume the bolometric corrections of Marconi et al. (2004). The use of the $6 \mu\text{m}$ continuum emission to infer L_{AGN} has the advantage that it is an independent measure of the intrinsic luminosity of the AGN, whilst the NL [OIV] emission arises from a similar region to that of [OIII] which was used for the selection of the sources considered here.

Twelve of our 14 sources have both M_{BH} estimates and $6 \mu\text{m}$ measurements. We find that our sample of AGNs are

¹¹ The MPA-JHU SDSS catalogue is maintained by a large collaboration of SDSS researchers and is a complementary dataset providing additional information for the SDSS-DR7 data-release including measurements of velocity dispersions, stellar masses, star-formation rates etc. It is available at <http://www.mpagarching.mpg.de/SDSS/>

spread over a wide-range of Eddington ratio, $\eta \approx 0.002$ – 0.3 (median ≈ 0.014 ; see Column 11 of Table 2); the five Compton-thick AGNs are at systematically higher Eddington ratios, $\eta \approx 0.01$ – 0.3 (median ≈ 0.2).¹² Similarly, we find that the well-studied local Compton-thick AGNs (Circinus, Mrk 3, NGC 1068 and NGC 6240) have a similar range in Eddington ratio, $\eta \approx 0.002$ – 1 (median ≈ 0.2). It is important to note the large uncertainties involved with calculating bolometric luminosities and subsequent Eddington ratios; the large scatter in the X-ray– $6\ \mu\text{m}$ relation combined with a possible Eddington ratio dependent bolometric correction (e.g., Vasudevan & Fabian 2007) could yield an uncertainty factor of the order $\gtrsim 10$ for the highest Eddington ratio sources. None of the AGNs in our sample appear to be Eddington-limited on the basis of the $6\ \mu\text{m}$ luminosity, and any uncertainties would apply equally to all of the AGNs considered here, hence our finding of systematically higher Eddington ratios for Compton-thick AGNs, to first-order, appears to be relatively robust. However, we suggest that this result may be driven by our selection of [OIII]-bright AGNs as well as our sensitivity towards the identification of Compton-thick AGNs. For example, with deeper X-ray data we may identify further Compton-thick AGNs in our sample which have lower values of η , and hence reducing the median Eddington ratio for the Compton-thick AGN subsample.

By comparison, for the total population of Type-2 AGNs identified from optical emission-line diagnostics in the SDSS, Heckman et al. (2004) find that based on the use of [OIII] emission to infer L_{AGN} , < 0.5 percent of Type-2 AGNs hosting SMBHs with $M_{\text{BH}} \approx 3 \times 10^7 M_{\odot}$ are accreting above $\eta \approx 0.1$; by contrast, we find that $\gtrsim 30$ percent of our sample have $\eta \gtrsim 0.1$. A particular advantage to a direct comparison with the study of Heckman et al. (2004) is that selection processes and biases are likely to be identical between both studies. Hence, these results suggest that, on average, the Compton-thick AGNs identified here may harbour some of the most rapidly growing black holes in the nearby Universe. This would further suggest that not taking account of Compton-thick AGNs in deep-field X-ray surveys may exclude the most rapid growth phases of SMBHs, as predicted by many theoretical models (e.g., Fabian 1999; Granato et al. 2006; Hopkins et al. 2008).

5 CONCLUSIONS

We have presented a sample of 14 local ($z \sim 0.03$ – 0.2) X-ray undetected optical AGNs selected from the large overlap region between the SDSS-DR7 and 2XMMi catalogues. These sources were selected as candidate Compton-thick AGNs on the basis of their X-ray–[OIII] emission line ratios (i.e., $f_X/f_{\text{[OIII]}} < 1.0$; e.g., Bassani et al. 1999; see Section 2). We have employed a suite of optical (e.g., [OIII] emission-line) and mid-IR (e.g., [OIV] emission-line; $6\ \mu\text{m}$ AGN continuum) diagnostics to infer the intrinsic AGN luminosity in these sources. Assuming any deficit in X-ray flux compared to these estimates is due to Compton-thick absorption, we

assess the ubiquity of Compton-thick AGN activity in the nearby Universe. Our main findings are the following:

(1) Using *Spitzer*-IRS low resolution spectroscopy, we find that six of our 14 candidate Compton-thick AGNs have $\gtrsim 3\sigma$ detections of [Nev] and all 14 have $\gtrsim 3\sigma$ detections of [OIV]. We performed mid-IR spectral decompositions of our sample to establish $6\ \mu\text{m}$ AGN continuum luminosities. Using established X-ray to mid-IR continuum and emission-line relationships, we infer the intrinsic X-ray luminosity of these AGNs and conservatively find that 6/14 ($\approx 43 \pm 21$ percent) of the sources in our sample appear to be heavily obscured with $N_H \gtrsim 1.5 \times 10^{24}\ \text{cm}^{-2}$ (i.e., are Compton-thick AGNs). See sections 3.3, 3.4 and 4.1.

(2) We used our results to infer the ubiquity of Compton-thick AGNs in our SDSS–2XMMi parent sample. We predict that on the basis of the analyses presented here that at least $\gtrsim 20$ percent of the 334 optical Type-2 AGNs in the SDSS-DR7 at $z \sim 0.03$ – 0.2 are obscured by Compton-thick material. This implies a space-density of $\log(\Phi) \gtrsim -4.9\ \text{Mpc}^{-3}$ for Compton-thick AGNs with $L_X \gtrsim 10^{42}\ \text{erg s}^{-1}$ at $z \sim 0.1$, which we suggest may be consistent with the number density of Compton-thick AGNs predicted by XRB synthesis models when accounting for all of our sample selection biases. See sections 4.1 and 4.2.

(3) We establish that the Compton-thick AGNs identified in our sample appear to be rapidly accreting. Using $6\ \mu\text{m}$ continuum luminosity to infer the L_{AGN} and the stellar velocity dispersion to estimate M_{BH} , we find systematically higher Eddington ratios for the most conservatively identified Compton-thick AGNs ($\eta \approx 0.2$). By comparison to studies of local Type-2 AGNs with similar SMBH masses ($M_{\text{BH}} \approx 3 \times 10^7 M_{\odot}$ e.g., Heckman et al. 2004), we find that Compton-thick AGNs selected in the SDSS may harbour some of the most rapidly growing black holes in the nearby Universe ($z \sim 0.1$). However, this result may be driven by our Compton-thick AGN identification process. See section 4.3.

In summary, we have established that approximately half of these sources have optical and mid-IR AGN indicators consistent with their observed X-ray emission being heavily obscured by Compton-thick material. Indirect multi-wavelength analyses, such as those employed here, are currently the most practical and reliable technique to identify Compton-thick AGNs which are 2–3 orders of magnitude further down the L_X – z plane than can be achieved using X-ray spectroscopy alone. Using the next generation of X-ray satellites (e.g., *NuStar*; *IXO*; *WFXT*), high-quality X-ray spectroscopy and $E > 10\ \text{keV}$ detections will allow us to directly and unambiguously identify which of these sources are Compton-thick AGNs.

ACKNOWLEDGMENTS

We thank the anonymous referee for their considered and thorough report which has improved the quality of this paper. We would like to acknowledge useful conversations with J Geach and T Roberts. We thank R Gilli and E Treister for kindly providing the XRB space density tracks. We also thank the Science & Technologies Facilities Council (ADG; RCH), the Royal Society (DMA) and the Leverhulme Trust

¹² We note that when using [OIV] emission to infer L_{AGN} , to first-order, we find a similar result (i.e., systematically higher Eddington ratios for the Compton-thick AGNs).

(DMA; JRM) for funding. This research has made use of the Sloan Digital Sky Survey data archive and the NASA *Spitzer* Space Telescope which is operated by the Jet Propulsion Laboratory, California Institute of Technology under contract with the National Aeronautics and Space Administration. This research has also made use of data obtained from the Leicester Database and Archive Service at the Department of Physics and Astronomy, Leicester University, UK.

REFERENCES

- Abazajian K. N., et al. 2009, *ApJS*, 182, 543
- Aird J., Nandra K., Laird E. S., Georgakakis A., Ashby M. L. N., Barmby P., Coil A. L., Huang J., Koekemoer A. M., Steidel C. C., Willmer C. N. A., 2010, *MNRAS*, 401, 2531
- Akylas A., Georgantopoulos I., 2009, *A&A*, 500, 999
- Alexander D. M., Bauer F. E., Brandt W. N., Schneider D. P., Hornschemeier A. E., Vignali C., Barger A. J., Broos P. S., Cowie L. L., Garmire G. P., Townsley L. K., Bautz M. W., Chartas G., Sargent W. L. W., 2003, *AJ*, 126, 539
- Alexander D. M., Brandt W. N., Hornschemeier A. E., Garmire G. P., Schneider D. P., Bauer F. E., Griffiths R. E., 2001, *AJ*, 122, 2156
- Alexander D. M., Chary R., Pope A., Bauer F. E., Brandt W. N., Daddi E., Dickinson M., Elbaz D., Reddy N. A., 2008, *ApJ*, 687, 835
- Alonso-Herrero A., Ward M. J., Kotilainen J. K., 1997, *MNRAS*, 288, 977
- Awaki H., Koyama K., Inoue H., Halpern J. P., 1991, *PASJ*, 43, 195
- Baldwin J. A., Phillips M. M., Terlevich R., 1981, *PASP*, 93, 5
- Barger A. J., Cowie L. L., Capak P., Alexander D. M., Bauer F. E., Fernandez E., Brandt W. N., Garmire G. P., Hornschemeier A. E., 2003, *AJ*, 126, 632
- Bassani L., Dadina M., Maiolino R., Salvati M., Risaliti G., della Ceca R., Matt G., Zamorani G., 1999, *ApJS*, 121, 473
- Bauer F. E., Yan L., Sajina A., Alexander D. M., 2010, *ApJ*, 710, 212
- Brandl B. R., Bernard-Salas J., Spoon H. W. W., Devost D., Sloan G. C., et al. 2006, *ApJ*, 653, 1129
- Brusa M., Civano F., Comastri A., Miyaji T., Salvato M., et al. 2010, *ApJ*, 716, 348
- Cardelli J. A., Clayton G. C., Mathis J. S., 1989, *ApJ*, 345, 245
- Carrera F. J., Ebrero J., Mateos S., Ceballos M. T., Corral A., Barcons X., Page M. J., Rosen S. R., Watson M. G., Tedds J. A., Della Ceca R., Maccacaro T., Brunner H., Freyberg M., Lamer G., Bauer F. E., Ueda Y., 2007, *A&A*, 469, 27
- Comastri A., 2004, in A. J. Barger ed., *Supermassive Black Holes in the Distant Universe* Vol. 308 of *Astrophysics and Space Science Library*, Compton-Thick AGN: The Dark Side of the X-Ray Background. pp 245–+
- Della Ceca R., Severgnini P., Caccianiga A., Comastri A., Gilli R., Fiore F., Piconcelli E., Malaguti P., Vignali C., 2008, *Memorie della Societa Astronomica Italiana*, 79, 65
- Diamond-Stanic A. M., Rieke G. H., Rigby J. R., 2009, *ApJ*, 698, 623
- Donley J. L., Rieke G. H., Alexander D. M., Egami E., Pérez-González P. G., 2010, *ApJ*, 719, 1393
- Draine B. T., Li A., 2007, *ApJ*, 657, 810
- Ebrero J., Carrera F. J., Page M. J., Silverman J. D., Barcons X., Ceballos M. T., Corral A., Della Ceca R., Watson M. G., 2009, *A&A*, 493, 55
- Fabian A. C., 1999, *MNRAS*, 308, L39
- Ferrarese L., Merritt D., 2000, *ApJ*, 539, L9
- Fiore F., Brusa M., Cocchia F., Baldi A., Carangelo N., Ciliegi P., Comastri A., La Franca F., Maiolino R., Matt G., Molendi S., Mignoli M., Perola G. C., Severgnini P., Vignali C., 2003, *A&A*, 409, 79
- Fiore F., Puccetti S., Brusa M., Salvato M., Zamorani G., et al. 2009, *ApJ*, 693, 447
- Gallimore J. F., Yzaguirre A., Jakoboski J., Stevenosky M. J., Axon D. J., Baum S. A., Buchanan C. L., Elitzur M., Elvis M., O’Dea C. P., Robinson A., 2010, *ApJS*, 187, 172
- Gebhardt K., Bender R., Bower G., Dressler A., Faber S. M., Filippenko A. V., Green R., Grillmair C., Ho L. C., Kormendy J., Lauer T. R., Magorrian J., Pinkney J., Richstone D., Tremaine S., 2000, *ApJ*, 539, L13
- Georgantopoulos I., Akylas A., Georgakakis A., Rowan-Robinson M., 2009, *A&A*, 507, 747
- Ghisellini G., Haardt F., Matt G., 1994, *MNRAS*, 267, 743
- Giacconi R., Zirm A., Wang J., Rosati P., Nonino M., Tozzi P., Gilli R., Mainieri V., Hasinger G., Kewley L., Bergeron J., Borgani S., Gilmozzi R., Grogin N., Koekemoer A., Schreier E., Zheng W., Norman C., 2002, *ApJS*, 139, 369
- Gilli R., Comastri A., Hasinger G., 2007, *A&A*, 463, 79
- Goulding A. D., 2010, Ph D. thesis, University of Durham, U.K.
- Goulding A. D., Alexander D. M., 2009, *MNRAS*, 398, 1165
- Goulding A. D., Alexander D. M., Lehmer B. D., Mullaney J. R., 2010, *MNRAS*, 406, 597
- Granato G. L., Silva L., Lapi A., Shankar F., De Zotti G., Danese L., 2006, *MNRAS*, 368, L72
- Greene J. E., Ho L. C., 2007, *ApJ*, 667, 131
- Heckman T. M., Kauffmann G., Brinchmann J., Charlot S., Tremonti C., White S. D. M., 2004, *ApJ*, 613, 109
- Heckman T. M., Ptak A., Hornschemeier A., Kauffmann G., 2005, *ApJ*, 634, 161
- Hickox R. C., Markevitch M., 2006, *ApJ*, 645, 95
- Hickox R. C., Markevitch M., 2007, *ApJ*, 661, L117
- Higdon S. J. U., Devost D., Higdon J. L., Brandl B. R., Houck J. R., Hall P., Barry D., Charmandaris V., Smith J. D. T., Sloan G. C., Green J., 2004, *PASP*, 116, 975
- Hopkins P. F., Hernquist L., Cox T. J., Kereš D., 2008, *ApJS*, 175, 356
- Houck J. R., Roellig T. L., et al. 2004, *ApJS*, 154, 18
- Kauffmann G., Heckman T. M., Tremonti C., Brinchmann J., Charlot S., White S. D. M., Ridgway S. E., Brinkmann J., Fukugita M., Hall P. B., Ivezić Ž., Richards G. T., Schneider D. P., 2003, *MNRAS*, 346, 1055
- Kauffmann G., Heckman T. M., White S. D. M., Charlot S., Tremonti C., Brinchmann J., Bruzual G., Peng E. W., Seibert M., Bernardi M., et al. 2003, *MNRAS*, 341, 33
- Kewley L. J., Dopita M. A., Sutherland R. S., Heisler C. A., Trevena J., 2001, *ApJ*, 556, 121
- Kormendy J., Richstone D., 1995, *ARA&A*, 33, 581

- LaMassa S. M., Heckman T. M., Ptak A., Hornschemeier A., Martins L., Sonnentrucker P., Tremonti C., 2009, *ApJ*, 705, 568
- Levenson N. A., Weaver K. A., Heckman T. M., Awaki H., Terashima Y., 2004, *ApJ*, 602, 135
- Luo B., Bauer F. E., Brandt W. N., Alexander D. M., Lehmer B. D., Schneider D. P., Brusa M., Comastri A., Fabian A. C., et al. 2008, *ApJS*, 179, 19
- Lutz D., Maiolino R., Spoon H. W. W., Moorwood A. F. M., 2004, *A&A*, 418, 465
- Magorrian J., Tremaine S., Richstone D., Bender R., Bower G., Dressler A., Faber S. M., Gebhardt K., Green R., Grillmair C., Kormendy J., Lauer T., 1998, *AJ*, 115, 2285
- Maiolino R., Comastri A., Gilli R., Nagar N. M., Bianchi S., Böker T., Colbert E., Krabbe A., Marconi A., Matt G., Salvati M., 2003, *MNRAS*, 344, L59
- Maiolino R., Salvati M., Bassani L., Dadina M., della Ceca R., Matt G., Risaliti G., Zamorani G., 1998, *A&A*, 338, 781
- Maiolino R., Shemmer O., Imanishi M., Netzer H., Oliva E., Lutz D., Sturm E., 2007, *A&A*, 468, 979
- Marconi A., Risaliti G., Gilli R., Hunt L. K., Maiolino R., Salvati M., 2004, *MNRAS*, 351, 169
- Matt G., Brandt W. N., Fabian A. C., 1996, *MNRAS*, 280, 823
- Matt G., Fabian A. C., Guainazzi M., Iwasawa K., Bassani L., Malaguti G., 2000, *MNRAS*, 318, 173
- Meléndez M., Kraemer S. B., Armentrout B. K., Deo R. P., Crenshaw D. M., Schmitt H. R., Mushotzky R. F., Tueller J., Markwardt C. B., Winter L., 2008, *ApJ*, 682, 94
- Meléndez M., Kraemer S. B., Schmitt H. R., Crenshaw D. M., Deo R. P., Mushotzky R. F., Bruhweiler F. C., 2008, *ApJ*, 689, 95
- Mulchaey J. S., Koratkar A., Ward M. J., Wilson A. S., Whittle M., Antonucci R. R. J., Kinney A. L., Hurt T., 1994, *ApJ*, 436, 586
- Mullaney J. R., Alexander D. M., Huynh M., Goulding A. D., Frayer D., 2010, *MNRAS*, 401, 995
- Netzer H., Mainieri V., Rosati P., Trakhtenbrot B., 2006, *A&A*, 453, 525
- Norman C., Hasinger G., Giacconi R., Gilli R., Kewley L., Nonino M., Rosati P., Szokoly G., Tozzi P., Wang J., Zheng W., Zirm A., Bergeron J., Gilmozzi R., Grogin N., Koekemoer A., Schreier E., 2002, *ApJ*, 571, 218
- Osterbrock D. E., Ferland G. J., 2006, *Astrophysics of gaseous nebulae and active galactic nuclei. Astrophysics of gaseous nebulae and active galactic nuclei*, 2nd. ed. by D.E. Osterbrock and G.J. Ferland. Sausalito, CA: University Science Books, 2006
- Panessa F., Bassani L., 2002, *A&A*, 394, 435
- Panessa F., Bassani L., Cappi M., Dadina M., Barcons X., Carrera F. J., Ho L. C., Iwasawa K., 2006, *A&A*, 455, 173
- Rees M. J., 1984, *ARA&A*, 22, 471
- Risaliti G., Maiolino R., Salvati M., 1999, *ApJ*, 522, 157
- Satyapal S., Vega D., Dudik R. P., Abel N. P., Heckman T., 2008, *ApJ*, 677, 926
- Siebenmorgen R., Krügel E., 2007, *A&A*, 461, 445
- Soltan A., 1982, *MNRAS*, 200, 115
- Tommasin S., Spinoglio L., Malkan M. A., Fazio G., 2010, *ApJ*, 709, 1257
- Tozzi P., Gilli R., Mainieri V., Norman C., Risaliti G., Rosati P., Bergeron J., Borgani S., Giacconi R., Hasinger G., Nonino M., Streblyanska A., Szokoly G., Wang J. X., Zheng W., 2006, *A&A*, 451, 457
- Treister E., Krolik J. H., Dullemond C., 2008, *ApJ*, 679, 140
- Treister E., Urry C. M., Virani S., 2009, *ApJ*, 696, 110
- Tremaine S., Gebhardt K., Bender R., Bower G., Dressler A., Faber S. M., Filippenko A. V., Green R., Grillmair C., Ho L. C., Kormendy J., Lauer T. R., Magorrian J., Pinkney J., Richstone D., 2002, *ApJ*, 574, 740
- Ueda Y., Akiyama M., Ohta K., Miyaji T., 2003, *ApJ*, 598, 886
- Vasudevan R. V., Fabian A. C., 2007, *MNRAS*, 381, 1235
- Vignali C., Alexander D. M., Gilli R., Pozzi F., 2010, *MNRAS*, 404, 48
- Ward M. J., Geballe T., Smith M., Wade R., Williams P., 1987, *ApJ*, 316, 138
- Watson M. G., et al. 2009, *A&A*, 493, 339
- Weaver K. A., Meléndez M., Mushotzky R. F., Kraemer S., Engle K., Malumuth E., Tueller J., Markwardt C., Bergeha C. T., Dudik R. P., Winter L. M., Armus L., 2010, *ArXiv e-prints*
- Wild V., Heckman T., Sonnentrucker P., Groves B., Armus L., Schiminovich D., Johnson B., Martins L., LaMassa S., 2010, *ArXiv e-prints*
- Worsley M. A., Fabian A. C., Bauer F. E., Alexander D. M., Hasinger G., Mateos S., Brunner H., Brandt W. N., Schneider D. P., 2005, *MNRAS*, 357, 1281
- Yan R., Ho L. C., Newman J. A., Coil A. L., Willmer C. N. A., Laird E. S., Georgakakis A., Aird J., Barmby P., et al. 2010, *ArXiv e-prints*

This paper has been typeset from a $\text{\TeX}/\text{\LaTeX}$ file prepared by the author.